

QuaRK: A Quantum Reservoir Kernel for Time Series Learning

Abdallah Aaraba
 abdallah.aaraba@usherbrooke.ca
 Université de Sherbrooke
 Sherbrooke, Québec, Canada

Ola Ahmad
 Thales cortAIX Labs
 Montréal, Québec, Canada

Soumaya Cherkaoui
 Polytechnique Montréal
 Montréal, Québec, Canada

Shengrui Wang
 Université de Sherbrooke
 Sherbrooke, Québec, Canada

Abstract

Quantum reservoir computing offers a promising route for time series learning by modelling sequential data via rich quantum dynamics while the only training required happens at the level of a lightweight classical readout. However, studies featuring efficient and implementable quantum reservoir architectures along with model learning guarantees remain scarce in the literature. To close this gap, we introduce QuaRK, an end-to-end framework that couples a hardware-realistic quantum reservoir featurizer with a kernel-based readout scheme. Given a sequence of sample points, the reservoir injects the points one after the other to yield a compact feature vector from efficiently measured k -local observables using classical shadow tomography, after which a classical kernel-based readout learns the target mapping with explicit regularization and fast optimization. The resulting pipeline exposes clear computational knobs—circuit width and depth as well as the measurement budget—while preserving the flexibility of kernel methods to model nonlinear temporal functionals and being scalable to high-dimensional data. We further provide learning-theoretic generalization guarantees for dependent temporal data, linking design and resource choices to finite-sample performance, thereby offering principled guidance for building reliable temporal learners. Empirical experiments validate QuaRK and illustrate the predicted interpolation and generalization behaviours on synthetic β -mixing time series tasks.

Keywords

Quantum Reservoir Computing, Quantum Kernels, Time Series

1 Introduction

Time series learning is a cornerstone in numerous modern data mining pipelines where related tasks involve forecasting, classification, anomaly detection, and decision-making in dynamical environments [2, 4, 11]. The main challenge is not only fitting nonlinear temporal dependencies, but also doing so under practical limitations such as limited labeled data, computational budgets, and the need for stable representations when the underlying process exhibits dependence and nonstationary effects. In this direction, reservoir computing [15, 21] has been an attractive modeling approach as it delegates most of the representational burden to a rich dynamical system, while restricting training to a lightweight readout, which yields a favourable trade-off between expressivity and optimization cost.

Quantum reservoir computing (QRC) extends this paradigm by leveraging quantum dynamics to generate features for sequential inputs [5, 6, 12]. By injecting temporal data into a quantum system and subsequently learning a classical readout, QRC proposes a principled way of representing time series with potentially rich, compact internal quantum states. However, there are two obstacles that limit the adoption of this approach as a reliable data mining tool. The first concerns the fact that existing designs are either inconvenient to implement faithfully on hardware or rely on expensive measurement schemes [33, 43]. The second is that works on the subject often lack end-to-end frameworks that connect concrete, efficiently implementable QRC architectures to explicit learning-theoretic guarantees on the generalization capacity of such methods [7, 34].

To reduce this gap, we propose in this work an implementable QRC architecture called QuaRK that is systematically designed with scalability in mind. First, a Johnson–Lindenstrauss (JL) [29] projection decouples the quantum resources (quantum circuit width and depth) from the original data dimension, enabling the model to remain practical even in the case of high-dimensional inputs. Each time series point is projected to this dimension, yielding a different representation of the initial series with dimensionality matching the number of qubits of the chosen quantum system. Second, the projected coordinates are sequentially injected into the quantum system through simple parameterized rotations followed by a fixed, hardware-friendly entangling layer. Third, using the classical shadows strategy [20], the quantum reservoir is probed by simultaneously estimating expectation values of k -local observables. Finally, following a projected quantum kernel [19] philosophy for time series [1], the reservoir readout is learned within the reproducing kernel Hilbert space (RKHS) of a classical kernel function applied to the space of features generated by the quantum featurizer.

Model capacity is explicitly characterized in a probably approximately correct (PAC) fashion [29, 38]. In particular, we show that with a number of qubits lower-bounded by the data dimension (number of samples and desired time series length), one can perfectly learn a dataset constructed out of window subsequences of the studied time series. We follow this with an analysis of the generalization capacity of the model conducted on weakly dependent data. In this context, we show that the model exhibits good generalization on unseen data as we increase the number of dataset samples. This learning-theoretic analysis is further validated empirically, showing that the theory matches the empirical results. In summary, our main contributions are as follows:

- (1) We introduce an end-to-end quantum reservoir kernel learner (QUARK) that couples a hardware-realistic quantum reservoir featurizer with an RKHS kernel readout for temporal learning, while decoupling quantum resources from the data dimension to enable scalability.
- (2) We adopt an RKHS-based readout (kernel ridge regression-style) that enables fast closed-form training and interpretable regularization control, applied to a feature space generated via efficient measurement of the quantum reservoir featurizer using classical shadows.
- (3) We provide learning-theoretic guarantees for dependent temporal data that relate resource/design choices (projection dimension, reservoir size, multiplexing, measurement budget, and regularization) to finite-sample performance. This is further validated empirically on representative temporal learning tasks.

In what follows, Section 2 introduces the learning setup and background on temporal processes and quantum reservoirs, Section 3 presents the QUARK architecture and theoretical analysis, Section 4 reports empirical validation on β -mixing time series tasks, and Section 5 discusses conclusions and future directions.

2 Framework and background.

2.1 Notation

We denote by $\mathbb{Z}_- := \{\dots, -2, -1, 0\}$ the set of non-positive integers, by \mathbb{N} the non-negative integers, and for $m \in \mathbb{N}^*$ we write $[m] := \{1, \dots, m\}$; for any set \mathcal{A} , $|\mathcal{A}|$ denotes its cardinality. Random objects are written in uppercase (e.g. X_t, Y_t) and processes in bold roman (e.g. $\mathbf{X} = (X_t : t \in \mathbb{Z}_-)$, $\mathbf{IO} = ((X_t, Y_t) : t \in \mathbb{Z}_-)$), while a (finite) observed trajectory is written in bold lowercase, $\mathbf{x} = (x_t : t \in \mathbb{Z}_-) \in (\mathcal{I})^{\mathbb{Z}_-}$ with $x_t \in \mathcal{I} \subset \mathbb{R}^d$ and $y_t \in \mathcal{Y} \subset \mathbb{R}$; a length- w window ending at time τ is $X_\tau^w := (X_{\tau-w+1}, \dots, X_\tau) \in (\mathcal{I})^w$ with realization $\mathbf{x}_\tau^w = (x_{\tau-w+1}, \dots, x_\tau)$, and a windows dataset is $\mathcal{D} = \{(\mathbf{x}_i, y_i)\}_{i=1}^N$ (we use $\mathbb{E}_P[\cdot]$ and $\Pr(\cdot)$ for expectation/probability under the law P). For an n -qubit register, $\mathcal{H} := \mathbb{C}^{2^n}$, $\mathcal{S}(\mathcal{H})$ is the space of density operators, and $\mathcal{B}(\mathcal{H})$ is the space of bounded operators on \mathcal{H} ; we use Dirac notation, set $|+\rangle\langle+|^\otimes := \otimes_{i=1}^n |+\rangle\langle+|$, and write $\langle O \rangle_\rho := \text{Tr}[O\rho]$ for the expectation of an observable O . We write $\|\cdot\|_2$ for the Euclidean norm, and $\|\cdot\|_{\text{HS}}$, $\|\cdot\|_1$, and $\|\cdot\|_\infty$ for the Hilbert-Schmidt, trace, and operator norms, respectively. For spatial multiplexing with $R \geq 1$ sub-reservoirs we work on $\mathcal{H}^{\otimes R} := \bigotimes_{r=1}^R \mathcal{H}$ and $\mathcal{B}(\mathcal{H})^R := \mathcal{B}(\mathcal{H}^{\otimes R})$; with a mild abuse of notation, $\mathcal{S}(\mathcal{H})^R$ denotes the corresponding state space and, in particular, the product states $\bigotimes_{r=1}^R \rho^{(r)}$ with each $\rho^{(r)} \in \mathcal{S}(\mathcal{H})$. Finally, \mathcal{O} denotes the set of measured k -local observables, $m : \mathcal{S}(\mathcal{H})^R \rightarrow \mathbb{R}^{R|\mathcal{O}|}$ the moment map producing features $\Phi = m \circ H^T$, and κ is the Matérn kernel with RKHS \mathcal{H}_κ and norm $\|\cdot\|_\kappa$; K denotes the associated Gram matrix and λ_{reg} the Tikhonov regularization parameter.

2.2 Learning temporal data processes.

Let $\mathbf{IO} = ((X_t, Y_t) : t \in \mathbb{Z}_-)$, where $X_t \in \mathcal{I}$ and $Y_t \in \mathcal{Y}$, be a semi-infinite input/output stochastic process¹, with $\mathcal{I} \subset \mathbb{R}^d$ being some bounded measurable input set such that $\sup_{x \in \mathcal{I}} \|x\|_2 \leq Y_X$, and

¹The probability space $(\Omega, \mathcal{A}, \mathbb{P})$ is fixed for all random variables and processes.

$\mathcal{Y} \subset \mathbb{R}$ some bounded measurable real-valued output set satisfying $\sup_{y \in \mathcal{Y}} |y| \leq Y_Y$. We distinguish between the stochastic process and its realizations: the input/output process \mathbf{IO} is a random object defined on a fixed probability space, while a (finite) time series corresponds to a single observed trajectory of this process, from which we construct windows for learning. We consider the supervised learning problem where the task is to learn the data generating process (DGP) functional (map) H^* that assigns Y_0 to the process $\mathbf{X} = (X_t : t \in \mathbb{Z}_-)$: $Y_0 = H^*(\mathbf{X})$, where the process \mathbf{IO} is distributed according to some unknown distribution P [7, 14]. This problem is rooted in real-life processes (e.g., weather data) where we only have access to data up to date (with the most recent index being $t = 0$) and we'd like to make a prediction Y_0 from such historical data (e.g., tomorrow's temperature, after a one-step shift of the time index).

As is central to machine learning, approximating the unknown DGP functional H^* follows from a risk minimization procedure. The (statistical) risk, or generalization error, associated with a functional H is defined with respect to a fixed L -Lipschitz ($L > 0$) loss function $\ell : \mathbb{R} \times \mathbb{R} \rightarrow \mathbb{R}$ (e.g. squared error) as

$$R(H) := \mathbb{E}_P[\ell(H(\mathbf{X}), Y_0)]. \quad (1)$$

We are interested in learning H^* from the family \mathcal{F} of functionals satisfying the fading memory property (FMP) [32]. Intuitively, this property implies that if two time series $\mathbf{x}, \mathbf{x}' \in (\mathcal{I})^{\mathbb{Z}_-}$ are similar in their recent past (i.e., have similar values x_t and x'_t for times $t > t^*$ for some past time point $t^* \in \mathbb{Z}_-$), then their outputs $H^*(\mathbf{x})$ and $H^*(\mathbf{x}')$ will be close, even if \mathbf{x} is very different from \mathbf{x}' in the distant past ($t < t^*$).

Given a hypothesis class of functionals $C \subset \mathcal{F}$, the ultimate goal of the learning procedure consists in determining the functional H_C that exhibits minimal risk by solving

$$H_C = \arg \min_{H \in C} R(H). \quad (2)$$

It is worth mentioning that the broader the class C is, the more accurate the learning can be, hence the need for a rich (expressive) hypothesis class. Since the risk $R(H)$ depends on an unknown distribution P as well as on a semi-finite time series process \mathbf{X} , it is generally infeasible to solve the optimization in Eq. (2). To this end, one must come up with an empirical risk \hat{R} that does not deviate significantly from the true risk², i.e., a quantity $|R(H) - \hat{R}(H)|$ that is controllable and can be computed efficiently. The learning procedure then becomes minimization of the empirical risk, i.e. $\arg \min_{H \in C} \hat{R}(H)$.

2.3 Quantum reservoir computers.

Crucial to reservoir computers (RCs) [22] is the state-space evolution described as

$$\rho_t = T(\rho_{t-1}, x_t), \quad \text{for all } t \in \mathbb{Z}_-, \quad (3)$$

where $T : \mathcal{S} \times \mathcal{I} \rightarrow \mathcal{S}$ is called the evolution map, and $\mathcal{S} \subset \mathcal{B}$ is the state space of some normed space $(\mathcal{B}, \|\cdot\|)$. Quantum reservoir computers (QRCs) are an important class of RCs that leverage the

²Having a controllable $|R(H) - \hat{R}(H)|$ is what we mean by a good generalization.

state spaces of quantum systems [6]. Indeed, QRCs have as state space the set of quantum states described by the convex subset

$$\mathcal{S}(\mathcal{H}) = \{ \rho \in \mathcal{B}(\mathcal{H}) : \text{Tr}[\rho] = 1, \rho \succeq 0 \}, \quad (4)$$

where $\mathcal{B}(\mathcal{H})$ is the space of bounded linear operators on the Hilbert space $\mathcal{H} = \mathbb{C}^{2^n}$ of an n -qubit quantum system. Unless otherwise stated, we mainly consider the Hilbert–Schmidt (HS) norm (i.e., the Schatten-2 norm) $\|\Psi\|_{\text{HS}} = \sqrt{\text{Tr}[\Psi^\dagger \Psi]}$, $\Psi \in \mathcal{B}(\mathcal{H})$ as the norm on $\mathcal{B}(\mathcal{H})$. Furthermore, at each time step, the state of a QRC is represented by a quantum state, while the quantum dynamics of the reservoir are described by a time-evolution map on the same quantum system (see [16] for details). Time-evolution maps on a quantum system are linear maps that are completely positive and trace-preserving (CPTP). For each fixed input $x_t \in \mathbb{R}^d$, the induced map $T(\cdot, x_t) : \mathcal{S}(\mathcal{H}) \rightarrow \mathcal{S}(\mathcal{H})$ is CPTP, and the state evolution is given by $\rho_t = T(\rho_{t-1}, x_t)$.

A QRC induces an inner filter, an inner-reservoir functional, and an outer-reservoir functional, defined respectively as

$$\begin{aligned} U^T : (\mathcal{I})^{\mathbb{Z}_-} &\longrightarrow (\mathcal{S}(\mathcal{H}))^{\mathbb{Z}_-}, & \mathbf{x} &\mapsto (T(s_{t-1}, x_t) : t \in \mathbb{Z}_-) \\ H^T : (\mathcal{I})^{\mathbb{Z}_-} &\longrightarrow (\mathcal{S}(\mathcal{H})), & \mathbf{x} &\mapsto U^T(\mathbf{x})_0 \\ H_h^T : (\mathcal{I})^{\mathbb{Z}_-} &\longrightarrow \mathbb{R}, & \mathbf{x} &\mapsto h \circ H^T(\mathbf{x}), \end{aligned} \quad (5)$$

where $h : \mathcal{S}(\mathcal{H}) \rightarrow \mathbb{R}$ is some readout function that combines a measurement scheme conducted on the quantum system with some classical post-processing.

There are two properties that are crucial in reservoir computing: the echo state property (ESP) and the fading memory property (FMP). The first, ESP, is satisfied when for every sequence $\mathbf{x} \in (\mathcal{I})^{\mathbb{Z}_-}$ there exists a sequence of states $(\rho_t : t \in \mathbb{Z}_-)$ that satisfies the relation in Eq. (3) for each $t \in \mathbb{Z}_-$, and such a solution is unique. The ESP has attracted a lot of attention in the literature on reservoir computing [22] because it gives the system a function-like definition where, for each input sequence, there is a single output sequence. The second property, on the other hand, states that a reservoir computer satisfies the FMP when its functional H_h^T satisfies it in the sense described in the second paragraph of Section 2.2. Combined together, these properties imply that a state ρ_t at time t depends less and less on earlier states ρ_{t-w} as we increase w . We will leverage this to show that the reservoir’s initial state becomes increasingly irrelevant to the output as the reservoir processes more and more time points.

An interesting family of reservoir computers is that of evolution maps T that are strictly contractive in their first argument:

$$\|T(\rho, x) - T(\rho', x)\| \leq \lambda \|\rho - \rho'\|, \text{ for all } \rho, \rho' \in \mathcal{S}, \quad (6)$$

where $\lambda \in (0, 1)$. This is of interest because any reservoir of this form automatically satisfies both the ESP and the FMP [15, 32]. Subsequently, in Section 3.1, we propose a design of quantum reservoirs satisfying this condition, which leads to a principled hypothesis class \mathcal{C}_R of functionals that we leverage to approximate an unknown DGP functional $H^* \in \mathcal{F}$.

3 Methodology

In this section, we present the end-to-end QUARK pipeline. In Section 3.1, we introduce our quantum reservoir embedding pipeline. Section 3.2 outlines how the reservoir is read out efficiently to form

feature vectors and how these are lifted into an RKHS for learning. Section 3.3 describes how the resulting kernel-based readout is classically trained. Finally, Section 3.4 analyzes, in a PAC-style fashion, the link between design/resource choices and finite-sample performance on weakly dependent data.

3.1 Quantum reservoir embedding

Although we described the machine learning problem in Section 2.2 as that concerning learning the mapping $H^* : \mathbf{X} \mapsto Y_0$, in reality we do not have a dataset of time series samples $\mathbf{x} \in (\mathcal{I})^{\mathbb{Z}_-}$ to train on. All we have is a single time series, i.e. a single realization of the process \mathbf{X} , which we must leverage to approximate the unknown H^* . To this end, we adopt the windows-based learning approach discussed in [14] to form an (artificial) windows dataset $\mathcal{D} = \{(\mathbf{x}_1, y_1), \dots, (\mathbf{x}_N, y_N)\}$, where each window is a lookback sequence \mathbf{x} of the form $\mathbf{x} = (x_{\tau-w+1}, \dots, x_\tau) \in (\mathcal{I})^w$ along with its label $y = y_\tau$ for some $\tau \in \mathbb{Z}_-$. We override the definition of the functional $H^T(\cdot)$, which was initially defined to accept semi-infinite inputs, with a definition of $H^T(\mathbf{x})$ for a given window \mathbf{x} that starts from an initial state $\rho_{\tau-w}$, evolves the reservoir with respect to inputs $x_t \in \mathbf{x}$, and returns the output state ρ_τ at the end of the evolution.

3.1.1 Projection. Let $n \in \mathbb{N}$ be the number of qubits chosen by the user and let $\mathbf{x} \in \mathcal{D}$. To make our model parameters independent of the data dimension, which is a key property for allowing scalability with potentially high dimensions d , we first project each input $x \in \mathbf{x}$ into another representation $z \in \mathbb{R}^n$ using a Johnson–Lindenstrauss (JL) data projection with a linear projection matrix $\Pi \in \mathbb{R}^{n \times d}$ so that $z = \Pi x$. We use a random matrix projection Π distributed according to the Gaussian JL distribution [8]

$$\Pi = (\Pi_{ij})_{i,j} \in \mathbb{R}^{n \times d}, \quad \Pi_{ij} \stackrel{\text{i.i.d.}}{\sim} \mathcal{N}(0, \frac{1}{n}). \quad (7)$$

Such a projection is deliberately chosen to yield low-distortion embeddings, so that the (Euclidean) distances between all points in the dataset—i.e. the set $\mathcal{P} := \bigcup_{i=1}^N \mathbf{x}_i \subset \mathbb{R}^d$ of cardinality at most wN —are nearly preserved. Importantly, one can show that if the number of qubits satisfies $n = \Omega(\epsilon_{\text{pr}}^{-2} \log(\frac{wN}{\delta}))$ for some error tolerance and failure probability $\epsilon_{\text{pr}}, \delta \in (0, 1)$, then for all $u, v \in \mathcal{P}$, we have

$$(1 - \epsilon_{\text{pr}}) \|u - v\|_2^2 \leq \|\Pi u - \Pi v\|_2^2 \leq (1 + \epsilon_{\text{pr}}) \|u - v\|_2^2, \quad (8)$$

with probability at least $1 - \delta$ by the standard JL lemma (see Theorem 2.1 in [41]). This observation is later leveraged to show effective learning with our reservoir computer (see Section 3.4.1).

3.1.2 Quantum reservoir architecture. For the QR architecture, we adopt a design that adheres to the family of quantum reservoirs called contracted-encoding quantum channels (CEQC) as introduced in [26]. Such a design is interesting for numerous reasons, the main one being its automatic satisfaction of the FMP and ESP. These channels are defined as CPTP maps $T : \mathcal{S}(\mathcal{H}) \times \mathcal{I} \rightarrow \mathcal{S}(\mathcal{H})$ that lead to state-space transformations of the form

$$\rho_t = T(\rho_{t-1}, x_t) := \mathcal{E} \circ \mathcal{J}(\rho_{t-1}, x_t), \quad (9)$$

where $\mathcal{E} : \mathcal{S}(\mathcal{H}) \rightarrow \mathcal{S}(\mathcal{H})$ is a strictly contractive map, and $\mathcal{J} : \mathcal{S}(\mathcal{H}) \times \mathcal{I} \rightarrow \mathcal{S}(\mathcal{H})$ is a CPTP map that encodes the input information. It is worth mentioning that quantum reservoirs defined

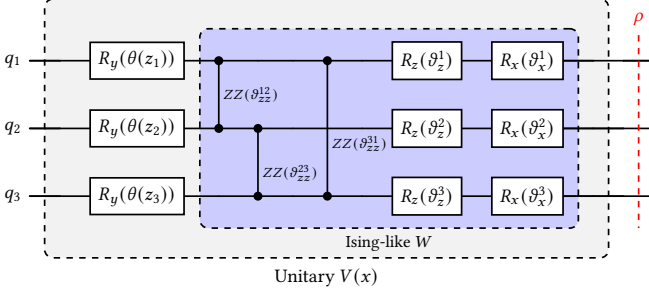


Figure 1: Circuit for the unitary evolution block $V(x)$ on three qubits with ring connectivity. First, classical features are encoded via single-qubit angle encoding $R_y(\theta(z_j))$ on each q_j . Then the Ising-like unitary W (Eq. (11)) is shown as ZZ couplings on the edges $(1, 2)$, $(2, 3)$, and $(3, 1)$, followed by local rotations $R_z(\theta_z)$ and $R_x(\theta_x)$.

by CPTP maps of this form encompass numerous architectures in the QRC literature, such as quantum circuits with noise [24, 39], reset-rate channels [6, 31], mid-circuit measurements [18, 42], and compositions of a dissipative channel with an amplitude encoding map [35]. The following paragraphs present our design for both channels \mathcal{J} and \mathcal{E} .

Unitary evolution. After projecting an input x into $z = \Pi x$, we inject each component z_j of z into the circuit using R_y gates parametrized by angles $\theta(z_j) = \pi \cdot \tanh(z_j) \in [-\pi, \pi]$, followed by a global fixed unitary W , which realizes the evolution $\mathcal{J}(\rho, x) = V(x)\rho V(x)^\dagger$, where

$$V(x) := W \bigotimes_{j=1}^n R_y(\theta(z_j)) \quad (10)$$

as illustrated in Figure 1. Furthermore, given our quantum hardware topology (V, E) , where the vertices are our n qubits and E contains available edges between qubits of the form (i, j) , we realize the unitary W following the Ising-like, hardware-friendly design

$$W = \prod_{j \in V} R_x(\theta_x^j) \prod_{j \in V} R_z(\theta_z^j) \prod_{(i, j) \in E} R_{zz}(\theta_{zz}^{ij}), \quad (11)$$

where all parameters θ_\bullet are sampled i.i.d. uniformly from $(-\pi, \pi)$.

Contractive quantum channel \mathcal{E} . Let $\lambda \in (0, 1)$ be a contraction factor. We design the channel \mathcal{E} as the reset-rate channel

$$\mathcal{E}_\lambda : \mathcal{S}(\mathcal{H}) \longrightarrow \mathcal{S}(\mathcal{H}), \quad \rho \longmapsto \lambda \rho + (1 - \lambda) |+\rangle\langle+|^{\otimes n}. \quad (12)$$

As it is easy to check (with $\mathcal{E}_\lambda(\rho')$ in the first line below) that

$$\|\mathcal{E}_\lambda(\rho) - \mathcal{E}_\lambda(\rho')\|_{\text{HS}} \leq \lambda \|\rho - \rho'\|_{\text{HS}} \quad (13)$$

and $\|\mathcal{J}(\rho, x) - \mathcal{J}(\rho', x)\| \leq \|\rho - \rho'\|$,

we have $\|T(\rho, x) - T(\rho', x)\|_{\text{HS}} \leq \lambda \|\rho - \rho'\|_{\text{HS}}$. Hence, we adhere to the condition in the last paragraph of Section 2.3, thereby making our reservoir computer satisfy both the ESP and FMP³. Figure 2 illustrates how we realize such a reset-rate channel on our quantum circuit, where, controlled on a coin qubit c rotated by $R_y(\theta_\lambda)$ with $\theta_\lambda = 2 \arcsin \sqrt{1 - \lambda}$, we swap reservoir qubits with ancilla ones all initialized to $|+\rangle$. The convex formula in Eq. (12) is thus realized, as

³Notice also that our map $T = \mathcal{E}_\lambda \circ \mathcal{J}$ is by definition non-unital, i.e., $T(I, x) \neq I$, hence we ensure a non-pathological, non-trivial filter as discussed in Theorem 1 of [25].

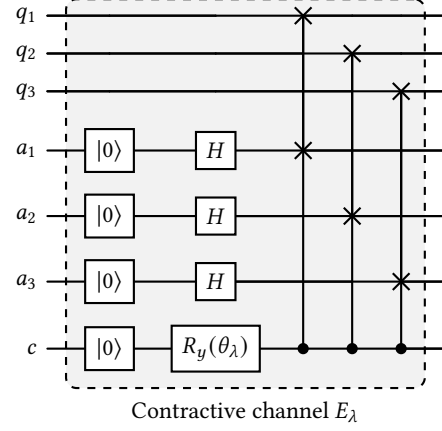


Figure 2: SWAP-dilation realization of the contractive channel E_λ acting on a 3-qubit reservoir state ρ (top wires). The ancilla register (middle wires) is reset to $|0\rangle$ and prepared in $|+\rangle^{\otimes 3}$ via Hadamards. A coin qubit (bottom wire) is reset and rotated by $R_y(\theta_\lambda)$, where $\theta_\lambda = 2 \arcsin \sqrt{1 - \lambda}$ so that $\Pr[c = 1] = 1 - \lambda$ and $\Pr[c = 0] = \lambda$. Conditioned on $c = 1$, controlled-SWAPs exchange each reservoir qubit q_i with its corresponding ancilla qubit a_i .

the coin c becomes superposed with probability $1 - \lambda$ of being in state $|1\rangle$. In what follows, we combine parameters θ_\bullet and λ into a single vector ϑ .

Quantum embedding of a window. Let $\mathbf{x} = (x_{\tau-w+1}, \dots, x_\tau)$ be a window of our time series. A consequence of using the reset-rate channel \mathcal{E}_λ is that, provided w is large enough, the state at which our quantum reservoir is initialized at time $\tau - w$ matters little to the output state ρ_τ (see the third paragraph of Section 2.3). Hence, by convention, we fix $\rho_{\tau-w} = |+\rangle\langle+|^{\otimes n}$ as the initial state of the reservoir at time $\tau - w$, and we process the inputs x_t step by step until reaching the output state ρ_τ , realizing the following reservoir evolution:

$$\rho_{\tau-w} \xrightarrow{T(\cdot, x_{\tau-w+1})} \rho_{\tau-w+1} \xrightarrow{T(\cdot, x_{\tau-w+2})} \dots \xrightarrow{T(\cdot, x_\tau)} \rho_\tau. \quad (14)$$

We refer to such a window embedding as $H^T(\mathbf{x}) \in \mathcal{S}(\mathcal{H})$, which maps the window \mathbf{x} to ρ_τ .

3.1.3 Increased expressivity via spatial multiplexing. As introduced in [36] and revised in [5, 6], we adopt the idea of spatial multiplexing to increase model expressivity. The idea is that, instead of using a single reservoir computer, we can use a set of $R \geq 1$ sub-reservoirs with the same architecture but different parameters. These sub-reservoirs are evolved independently (e.g., by running different quantum circuits with different parameters ϑ), so that for a single window \mathbf{x} we obtain a set of R different quantum states, thereby increasing the feature vector size and expressivity. We mathematically represent the resulting spatially multiplexed (SM) window embedding using the compact equivalent form

$$H^T : \mathbf{x} = (x_{\tau-w+1}, \dots, x_\tau) \longmapsto \bigotimes_{r=1}^R H^{Tr}(\mathbf{x}) := \rho_\tau^{(r)} \in \mathcal{S}(\mathcal{H})^R, \quad (15)$$

with T_r being the evolution map of sub-reservoir $r \in [R]$. In addition, the parameters ϑ_r are all sampled independently. Working with different contraction values λ_r is beneficial, as it yields different sub-functionals H^{T_r} each with a different fading-memory structure, thereby enriching model expressivity with respect to modeled memories⁴.

3.2 Reading out the reservoir

In this section, we describe the readout module. We first present an efficient classical shadows measurement scheme to form feature vectors from the reservoir state, then explain how a kernel-based RKHS readout is trained on these features.

3.2.1 Efficient measurement scheme. At the end of the reservoir, we read out each sub-reservoir state ρ_r by measuring a set of k -local observables denoted by O —in our experiments in Section 4, we set O to be the set of 2-local Pauli observables⁵. Such a choice is deliberately made so that measuring the sub-reservoirs can be efficiently realized. Indeed, we make use of the classical-shadow estimator [20], which states that one can simultaneously and efficiently estimate all moments $[\langle O \rangle_{\rho_r} : O \in O]$ up to error tolerance $\varepsilon_{\text{cs}} \in (0, 1)$ using only a number of circuit runs (classical snapshots) scaling as $O\left(\left(\frac{3}{2}\right)^k \varepsilon_{\text{cs}}^{-2} \log(|O|)\right)$ by employing random single-qubit Pauli basis measurements [20].

The moments are estimated using the median-of-means algorithm, as introduced in the seminal paper on classical shadows [20], which is more resistant to statistical fluctuations. In the end, our measurement scheme for the sub-reservoirs $m : \mathcal{S}(\mathcal{H})^R \rightarrow \mathbb{R}^{|O|}$ produces the feature vector

$$\Phi(\mathbf{x}) = m\left(H^T(\mathbf{x})\right) := \left[\langle O \rangle_{\rho_r^{(r)}} : O \in O, r \in [R]\right]^T \in \mathbb{R}^{|O|}, \quad (16)$$

where $H^T(\mathbf{x}) = \bigotimes_r \rho_r^{(r)}$. Subsequently, feature vectors of this kind form the inputs to the classical Matérn kernel we use in the following section.

3.2.2 RKHS readout. Let φ be a (unit-variance) Matérn covariance with smoothness and lengthscale parameters $v > 1$ and $\xi > 0$, respectively, defined as

$$\varphi(s) := \frac{2^{1-v}}{\Gamma(v)} \left(\sqrt{2v} \frac{s}{\xi}\right)^v K_v \left(\sqrt{2v} \frac{s}{\xi}\right), \quad (17)$$

where Γ is the gamma function, and K_v is the modified Bessel function of the second kind [13]. We then define our kernel function κ on $\mathcal{S}(\mathcal{H})^R$ as

$$\begin{aligned} \kappa : \mathcal{S}(\mathcal{H})^R \times \mathcal{S}(\mathcal{H})^R &\rightarrow \mathbb{R} \\ (\rho, \rho') &\mapsto \varphi\left(\|\rho - \rho'\|_2\right). \end{aligned} \quad (18)$$

Finally, the classical readout functions h we use are drawn from the reproducing kernel Hilbert space (RKHS) \mathcal{H}_κ of κ defined as the closure (inclusion of limit points) of the set of functions [17]

$$\mathcal{H}_\kappa^{(0)} := \left\{ h = \sum_{i=1}^{s_h} \alpha_i \kappa(\rho_i, \cdot) : \alpha_i \in \mathbb{R}, \rho_i \in \mathcal{S}(\mathcal{H}), s_h \in \mathbb{N} \right\}, \quad (19)$$

⁴It has been shown that the family of QRCs is universal in that of the functionals with the FMP [36].

⁵A Pauli observable $P = \sigma_1 \otimes \dots \otimes \sigma_n$, with $\sigma_i \in \{I, X, Y, Z\}$, is called k -local (or weight $\leq k$) if the index set $\{i \in [n] : \sigma_i \neq I\}$ has cardinality $\leq k$.

i.e., $\mathcal{H}_\kappa := \overline{\mathcal{H}_\kappa^{(0)}}$. We equip such an RKHS space with the norm defined for each $h \in \mathcal{H}_\kappa$ as $\|h\|_\kappa := \sqrt{\langle h, h \rangle_\kappa}$, with $\langle \cdot, \cdot \rangle_\kappa$ being the RKHS's inner-product [17].

This readout scheme adheres to the principle of projected quantum kernels [19], consisting of first measuring and then applying a kernel wrapper to the resulting feature vectors. Hence, our approach is a legitimate quantum kernel method applied to time series data. Additionally, we choose a Matérn profile because its RKHS exhibits a polynomial algebraic structure, which is required to preserve the polynomial-algebra structure induced by the spatial multiplexing design used to increase model expressivity [32].

3.3 Readout training with empirical risk minimization

Given a fixed quantum channel T , i.e. after sampling parameters ϑ , and fixing the number of qubits n and the number of sub-reservoirs R , we now show how the kernel-based readout h is trained. Let φ be a Matérn profile, as described in Eq. (17), parameterized by hyperparameters v and ξ . Suppose we have a (training) dataset of windows $\mathcal{D} = \{(\mathbf{x}_1, y_1), \dots, (\mathbf{x}_N, y_N)\}$ that contains window samples \mathbf{x}_i along with their labels $y_i \in \mathbb{R}$, obtained from some unknown functional H^* . We learn the best readout $h \in \mathcal{H}_\kappa$ following an empirical risk minimization scheme, where we minimize the empirical risk $\hat{R}_N(H_h^T)$ with respect to the dataset \mathcal{D} given by

$$\hat{R}_N(H_h^T) := \frac{1}{N} \sum_{i=1}^N \ell\left(H_h^T(\mathbf{x}_i), y_i\right), \quad (20)$$

with ℓ being the squared loss function⁶ $\ell(\hat{y}, y) := (\hat{y} - y)^2$.

The bias-variance tradeoff of the model is controlled by restricting the RKHS readout. Concretely, h is learned by minimizing the empirical risk while enforcing a norm budget $\|h\|_\kappa \leq \Lambda$. Such a constrained problem admits an equivalent Tikhonov-regularized formulation [37] where there exists a $\lambda_\lambda \geq 0$ (a Lagrange multiplier for the constraint $\|h\|_\kappa \leq \Lambda$) for which the solution of the norm-constrained empirical risk minimization satisfies

$$\arg \min_{h \in \mathcal{H}_\kappa(\Lambda)} \hat{R}_N(H_h^T) = \arg \min_{h \in \mathcal{H}_\kappa} \hat{R}_N(H_h^T) + \lambda_\lambda \|h\|_\kappa^2, \quad (21)$$

where $\mathcal{H}_\kappa(\Lambda)$ is the RKHS ball of radius Λ defined as

$$\mathcal{H}_\kappa(\Lambda) := \{h \in \mathcal{H}_\kappa : \|h\|_\kappa \leq \Lambda\} \quad (22)$$

By the representer theorem [17], the optimal readout admits the form $h(\cdot) = \sum_{i=1}^N \alpha_i \kappa(H^T(\mathbf{x}_i), H^T(\cdot))$. Training thus reduces to kernel ridge regression, where we solve a finite-dimensional linear system in α . The closed-form solution is given by

$$\alpha = (K + N\lambda I)^{-1} \mathbf{y}, \quad (23)$$

where K is the Gram matrix with elements $K_{ij} := \kappa(H^T(\mathbf{x}_i), H^T(\mathbf{x}_j))$ for the different windows $\mathbf{x}_i, \mathbf{x}_j \in \mathcal{D}$, and $\mathbf{y} := (y_1, \dots, y_N)^\top$ is the label vector.

3.4 Learning theoretic analysis

3.4.1 Effective task learning. In this section, we show that we can effectively learn the task functional under mild conditions on the quantum resources used. Let our dataset of windows be

⁶Other Lipschitz losses may be used as discussed in Section 2.2.

$\mathcal{D} = \{(\mathbf{x}_1, y_1), \dots, (\mathbf{x}_N, y_N)\}$. We argue as follows that, upon using a quantum reservoir computer with a number of qubits as low as $n = \Omega(\log(wN))$, we can, with high probability, achieve effective empirical learning. In this setting, we show in the following theorem that, in an idealized noiseless setting (as opposed to the noisy feature maps of Section 3.2.1), we obtain effective learning of the task at hand. The proof of such result can be found in Appendix A.1.

Theorem 1 (Effective learning). *Suppose a design of a quantum reservoir as described in Section 3.1 with a number of $R \geq 1$ sub-reservoirs, and let our readout scheme follow the kernel-based one described in Section 3.2. Let $\varepsilon_{\text{pr}}, \delta_{\text{pr}} \in (0, 1)$ be, respectively, an error tolerance and a failure probability parameter. Then, with a number of qubits as low as $n = \Omega\left(\varepsilon_{\text{pr}}^{-2} \log\left(\frac{wN}{\delta_{\text{pr}}}\right)\right)$, with probability at least $1 - \delta_{\text{pr}}$, there exists a value $\Lambda^* > 0$ such that for any constraint $\Lambda \leq \Lambda^*$, we have*

$$\min_{h \in \mathcal{H}_k(\Lambda)} \hat{R}_N(H_h^T) = O\left(\left(1 - \frac{\Lambda}{\Lambda^*}\right)^2\right). \quad (24)$$

Theorem 1 can be read as a capacity statement for the end-to-end functional H_h^T : for a fixed quantum featurizer, enlarging the RKHS norm constraint decreases the achievable training loss. This is made explicit in Eq. (24) by exhibiting a budget threshold (which depends on the Gram matrix) such that, once Λ is relaxed enough to approach Λ^* , the empirical risk can be driven arbitrarily close to zero. Therefore, under the stated qubit scaling (which leads to a JL projection preserving the finite window set's geometry with high probability), the kernel readout becomes expressive enough to interpolate the dataset under sufficiently weak regularization. The interpretation of this result should be solely that there exists an effective interpolation regime.

3.4.2 Generalization analysis on weakly-dependent data. Though Theorem 1 shows that empirical fit is achievable with modest quantum resources, it says nothing about how the empirical risk deviates from the true risk $R(H_h^T)$ as defined in Eq. (1), i.e., generalization is not guaranteed. Characterizing the generalization gap $|R(H_h^T) - \hat{R}_N(H_h^T)|$ is, in general, a non-trivial endeavour for time series data, as we do not necessarily have the required i.i.d. property for the window samples of our hookups dataset \mathcal{D} (between-window dependence may occur), which is often assumed by standard learning-theoretic analyses.

In our treatment, we provide a generalization characterization for the case where our data are weakly dependent and are sampled from a β -mixing process $\text{IO} = ((X_t, Y_t) : t \in \mathbb{Z}_-)$. In essence, a β -mixing process means that the “far past” of the sequence and the “far future” become more and more independent as we increase the temporal gap (formal definitions can be found in Appendix A.2). This property can be leveraged to enable coupling/blocking arguments that lead to generalization bounds similar to the i.i.d. case, with an explicit dependence-related penalty [28]. It is worth mentioning that this weak-dependence assumption encompasses a broad class of time series models used in practice, which are β -mixing under verifiable stability/ergodicity conditions, making our analysis applicable well beyond the i.i.d. setting [3, 9, 10].

We now describe how we construct a dataset that leads to our generalization guarantee. We observe a stationary input/output

process IO (see Section 2.2 for details). Then, a window \mathbf{x}_i is constructed as the realization of the sub-process $(X_{t_i-w+1}, \dots, X_{t_i})$ and is assigned a label y_i , the realization of Y_{t_i} . When windows overlap, dependence arises; hence, we instead select indices with stride $s = w + g$, where g is a controllable gap. Increasing g increases, in turn, the independence between windows for our β -mixing process. Sampling N windows while respecting stride s between consecutive windows is how we construct our dataset $\mathcal{D} = \{(\mathbf{x}_1, y_1), \dots, (\mathbf{x}_N, y_N)\}$, where we assume $t_1 > t_2 > \dots > t_N$ with $t_i - t_{i+1} = s$. We now present our generalization result for the β -mixing case the proof of which can be found in Appendix A.3.3.

Theorem 2 (Generalization on weakly-dependent data). *Consider $\text{IO} = ((X_t, Y_t) : t)$ as a stationary β -mixing process with bounded outputs $|Y_t| \leq Y_Y$. Fix a window length w and a gap g , and construct a strided windows dataset $\mathcal{D} = \{(\mathbf{x}_i, y_i)\}_{i=1}^N$ with stride $s = w + g$ (as in the paragraph above). Assume N is even and write $N = 2\mu$. Let T be a QR featurizer composed of R sub-reservoirs with contraction values $\{\lambda_r\}_{r=1}^R$, and let κ be the unit-variance Matérn kernel used in Section 3.2 (with parameters $v > 1$ and $\xi > 0$). Let \mathcal{O} be the set of measured k -local observables. Define $\lambda_\star := \max_{r \in [R]} \lambda_r$.*

Fix any $\delta \in (0, 1)$ such that

$$\delta > 4(\mu - 1)\beta_{\text{IO}}(g), \quad \delta' := \delta - 4(\mu - 1)\beta_{\text{IO}}(g) > 0. \quad (25)$$

Then, with probability at least $1 - \delta$, the following holds simultaneously for all $h \in \mathcal{H}_k(\Lambda)$:

$$\begin{aligned} |R(H_h^T) - \hat{R}_N(H_h^T)| &\leq \underbrace{4\sqrt{2} \frac{\Lambda(\Lambda + \Upsilon_Y)}{\sqrt{N}}}_{\text{(Rademacher term)}} + \underbrace{3(\Lambda + \Upsilon_Y)^2 \frac{\sqrt{\log(4/\delta')}}{\sqrt{N}}}_{\text{(mixing penalty)}} \\ &+ \underbrace{\frac{4\Lambda(\Lambda + \Upsilon_Y)}{\xi} \sqrt{\frac{vR|\mathcal{O}|}{v-1}} \lambda_\star^w}_{\text{(window truncation via contraction)}}. \end{aligned} \quad (26)$$

Theorem 2 provides a uniform high-probability bound on the generalization gap $|R(H_h^T) - \hat{R}_N(H_h^T)|$ for all readouts h within the RKHS ball $\mathcal{H}_k(\Lambda)$ trained on a strided windows dataset. The bound decomposes into three terms. First, a standard Rademacher complexity term of order $1/\sqrt{N}$, which penalizes model richness. Second, a dependence penalty that is also $O(1/\sqrt{N})$ but whose confidence level is effectively reduced by temporal dependence through $\delta' = \delta - 4(\mu - 1)\beta_{\text{IO}}(g)$; hence the need to choose a gap g large enough to reduce $\beta_{\text{IO}}(g)$. Third, a fading-memory remainder that decays geometrically with λ_\star^w , which penalizes the fact that the reservoir forgets information beyond the window horizon. Consequently, for a fixed design, increasing the number of windows N drives the first two terms to zero, while choosing w moderately large (or ensuring stronger contraction) makes the truncation term negligible. In practice, the gap g controls statistical dependence between windows, while w controls the approximation to the reservoir's infinite-memory dynamics, thereby yielding a clear bias-dependence-variance tradeoff.

4 Empirical validation

In this section, we provide empirical validation of our end-to-end QuARK model. The goal is to empirically support our two key

learning-theoretic guarantees outlined in our theoretical analysis. First, we study the capacity of our model to effectively learn the selected tasks by showing that the training mean-squared error decreases smoothly and reaches zero beyond a finite threshold as we sweep the readout complexity, thereby corroborating the existence of an interpolation regime for our method. Second, we study our model’s generalization capacity. Once trained in this effective-learning regime, we evaluate the out-of-sample performance of the model and demonstrate that the test error decreases as we increase the number of training windows, which aligns with the scaling suggested by our generalization bound. In order to keep the empirical study compact and highly interpretable, we focus on a synthetic β -mixing vector autoregressive moving average (VARMA) family and representative DGP functionals with varying complexity. The experiments were conducted using Qiskit [23], and the quantum circuits were simulated on a simulator using a machine with two Nvidia A100 GPUs. Code available here <https://github.com/abdoary/quark>.

4.1 Empirical set up

For all the experiments, we generate a multivariate input process $\mathbf{X} = (X_t)_{t \leq 0} \in (\mathcal{I})^{\mathbb{Z}_-}$, with $\mathcal{I} := (-1, 1)^d$ and $d = 3$, from a VARMA(p, q) recursion with $p = q = 3$ (to allow multistep dependencies), given as

$$Z_t = \sum_{i=1}^p \Phi_i Z_{t-i} + \Theta_0 \epsilon_t + \sum_{j=1}^q \Theta_j \epsilon_{t-j}, \quad X_t := \tanh(Z_t), \quad (27)$$

where (ϵ_t) are i.i.d. centered innovations, and the AR part satisfies the usual stability conditions to allow the β -mixing property (see Appendix B.1.1 for details). From a trajectory, we form supervised examples by sliding windows of length w , $\mathbf{X}_t := (X_{t-w+1}, \dots, X_t)$, along with a scalar label $Y_t \in \mathbb{R}$, with $w = 25$ and a stride $s = 100$ (i.e. gap $g = 75$). Labels are generated by fixed ground-truth fading-memory functionals $H^\star : (\mathcal{I})^{\mathbb{Z}_-} \rightarrow \mathbb{R}$, whose window-truncated versions H_w^\star are used so that $Y_t = H_w^\star(\mathbf{X}_t)$.

We consider three functionals (tasks) chosen with varying difficulty. The first and easiest task is a one-step forecasting functional $H_{\text{fore}}^\star(\mathbf{X}_t) := u^\top \mathbf{X}_{t+1}$, with $u \in \mathbb{R}^d$ defining a fixed projection, which depends linearly only on the immediate future. The second, more difficult task is an exponentially fading linear functional, which involves decaying memory over many lags in a linear fashion,

$$H_{\text{exp}}^\star(\mathbf{X}_t) := \sum_{k \geq 0} \alpha^k u^\top \mathbf{X}_{t-k}, \quad Y_t := H_{\text{exp}, w}^\star(\mathbf{X}_t) := \sum_{k=0}^{w-1} \alpha^k u^\top \mathbf{X}_{t-k}, \quad (28)$$

with $\alpha \in (0, 1)$, thereby requiring the learning model to aggregate information across the whole window while capturing the decaying importance. The final and most difficult task is related to a Volterra-type functional of order two, which adds quadratic cross-lag interactions to the fading memory term in Eq. (28),

$$H_{\text{vol}}^\star(\mathbf{X}_t) = \sum_{k \geq 0} \alpha^k u^\top \mathbf{X}_{t-k} + \frac{1}{2} \sum_{k \geq 0} \sum_{\ell \geq 0} \alpha^{k+\ell} (v^\top \mathbf{X}_{t-k})(v^\top \mathbf{X}_{t-\ell}), \quad (29)$$

with $v \in \mathbb{R}^d$ defining a fixed projection, and where $H_{\text{vol}, w}^\star$ is obtained by truncating $k, \ell \in \{0, \dots, w-1\}$.

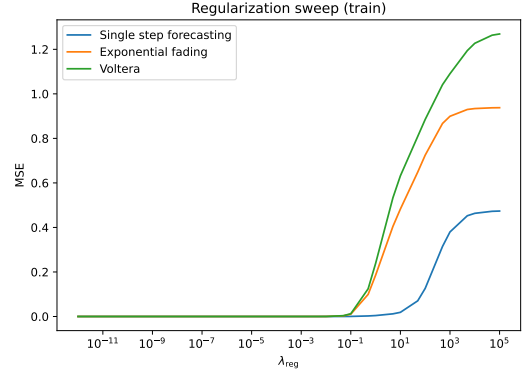


Figure 3: Training MSE versus the readout regularization λ_{reg} for the three functionals, featuring a sharp transition into the interpolation regime around $\lambda_{\text{reg}} \approx 10^{-1}$, where the curves reach numerical zero.

4.2 Learning theory validation

We used $n = 5$ qubits per sub-reservoir to align the empirical study with the projection-dimension guideline proposed in Section 3.1.1. This matches the prescribed scaling $n \approx \log(wN)$ for the JL projection dimension, with $w = 25$ and a maximum number of training windows of $N = 8000$. This choice is made for the two experiments below in order to fix the quantum featurizer complexity while probing the emergence of an interpolation regime by sweeping the readout norm budget and testing the generalization bound’s sample-size behavior by varying the number of training windows up to $N = 8000$.

Embeddings $H^T(\mathbf{X})$ are probed following the classical-shadows measurement strategy on the 2-local Pauli observable set. We perform 1000 measurement shots (classical snapshots) per circuit to construct the feature vector $m \circ H^T(\mathbf{X})$. A number of $R = 3$ independent sub-reservoirs are used to obtain a rich representational capacity. Throughout all the experiments, the architecture of each sub-reservoir is fixed to be the ring architecture and unitary pattern illustrated in Figure 1.

4.2.1 Effective learning validation. The first experiment validates the effective-learning prediction of our theoretical analysis in Section 3.4.1 by isolating a single control parameter: the readout complexity. Concretely, we fix all experimental choices, including the quantum featurizer, and we perform a sweep over the regularization parameter λ_{reg} (equivalently, a sweep over the RKHS norm budget Λ). Figure 3 reports the training MSE for each of the three tasks as a function of the regularization parameter. The key observation in this figure is the existence of a clear transition point into an interpolation regime, where, as we relax the constraint, the training error decreases and eventually reaches numerical zero in a smooth fashion. This is precisely what is predicted by Theorem 1: beyond a finite threshold, the readout hypothesis class becomes rich enough to push the empirical risk to zero. Furthermore, Figure 4 illustrates the fit on a subset of training windows in the interpolation regime, where we visualize predictions against ground-truth labels. This shows perfect fitting of the training dataset and highlights that the low training loss reported in Figure 3 is not merely an artifact of averaging.

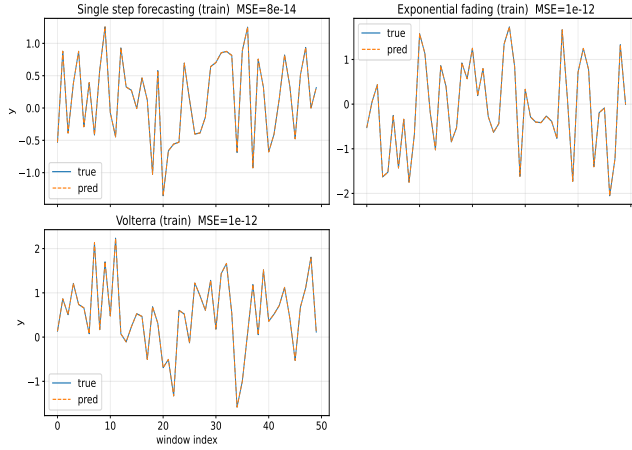


Figure 4: Predicted vs true labels on a subset of training windows for the three functionals from the interpolation regime. Numerical errors reach values of $MSE \in [10^{-14}, 10^{-12}]$ confirming perfect task learning.

4.2.2 Generalization guarantee validation. In this second experiment, we experimentally validate the claim made in Theorem 2. We first fix all modeling choices to a single configuration: same kernel, same quantum featurizer, and a single fixed readout regularization λ_{reg} chosen to be sufficiently relaxed. Then, we sweep the number of training windows N from 100 to $8 \cdot 10^3$, where for each value of N , we train the same kernel readout on the corresponding training subset and record the out-of-sample MSE on a fixed held-out test set. Figure 5 illustrates that the test error decreases as N increases across the three tasks, which aligns with the scaling predicted by the bound in Eq. (26). Importantly, the decay of the three curves follows the same $\frac{1}{\sqrt{N}}$ shape (up to additional constants), thereby validating the prediction made in Section 3.4.2. Furthermore, the ranking of the obtained test MSE values reflects the relative hardness of the functionals: the single-step forecasting functional yields the lowest values, followed by the exponential-fading and Volterra functionals.

5 Conclusion

In this paper, we introduced QUARK, an end-to-end quantum-classical learner for time-series prediction that couples a contractive quantum reservoir featurizer with a kernel-based RKHS readout. Our pipeline operates on windowed inputs and leverages a Johnson–Lindenstrauss projection to decouple the required quantum resources from the ambient data dimension. To enhance expressiveness while keeping the quantum component hardware-realistic, QUARK relies on spatial multiplexing through multiple sub-reservoirs, and forms compact feature vectors by estimating families of k -local Pauli observables using classical-shadow tomography; these features are then learned with kernel ridge regression, where regularization provides an explicit and interpretable control of readout complexity.

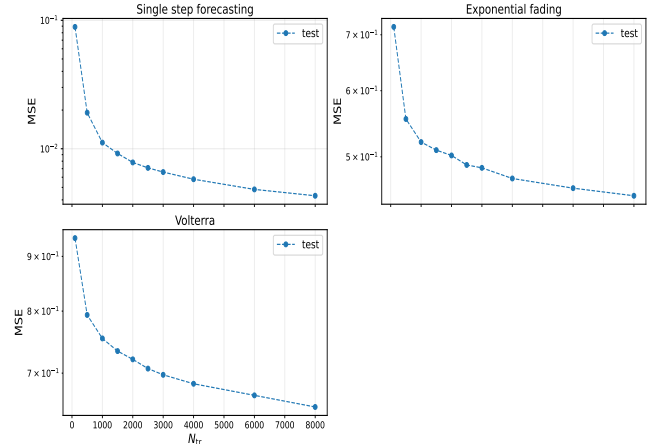


Figure 5: Test MSE vs training-set size N reported for the three tasks, obtained by sweeping N while keeping the other experimental choices, and reported for a same held-out test split.

On the learning-theoretic side, we connected these design choices to finite-sample performance under weak dependence. We established an effective interpolation regime, showing that once the embedding preserves enough geometry (via the prescribed projection/qubit scaling), relaxing the RKHS constraint yields a class rich enough to drive the empirical risk to (numerically) zero. We then provided a PAC-style generalization result for strided windows extracted from a stationary β -mixing process, recovering i.i.d.-like rates up to an explicit dependence penalty; empirically, our synthetic β -mixing VARMA benchmarks confirm the interpolation transition and the expected test-error decay when sweeping the number of training windows with a fixed featurizer and kernel.

Several directions remain to further consolidate QUARK as a practical and hardware-relevant methodology. A natural next step is to sharpen the analysis under realistic noise and finite-shot effects, and to make the tradeoffs between measurement budget, observable locality k , multiplexing, and accuracy more explicit. Finally, more systematic tuning of the design choices (projection dimension/qubit count, sub-reservoir count, observable families, and Matérn hyperparameters) and validation on higher-dimensional, longer-memory, and nonstationary real-world time series will clarify when each component of the pipeline (projection, contraction, multiplexing, and kernel readout) yields the strongest gains.

References

- [1] Abdallah Aaraba, Soumaya Cherkaoui, Ola Ahmad, Jean-Frédéric Laprade, Olivier Nahman-Lévesque, Alexis Vieloszynski, and Shengrui Wang. 2024. QuaCK-TSF: Quantum-Classical Kernelized Time Series Forecasting. 1628–1638 pages. doi:10.1109/qce60285.2024.00190
- [2] Abdallah Aaraba, Shengrui Wang, and Jean-Marc Patenaude. 2024. FR³LS: A Forecasting Model with Robust and Reduced Redundancy Latent Series. In *Pacific-Asia Conference on Knowledge Discovery and Data Mining*. Springer, 3–15. doi:10.1007/978-981-97-2266-2_1
- [3] Marine Carrasco and Xiaohong Chen. 2002. Mixing and Moment Properties of Various GARCH and Stochastic Volatility Models. *Econometric Theory* 18, 1 (Feb. 2002), 17–39. doi:10.1017/s0266466602181023
- [4] Varun Chandola, Arindam Banerjee, and Vipin Kumar. 2009. Anomaly detection: A survey. *Comput. Surveys* 41, 3, Article 15 (July 2009), 58 pages. doi:10.1145/1541880.1541882

[5] Jiayin Chen and Hendra I. Nurdin. 2019. Learning nonlinear input–output maps with dissipative quantum systems. *Quantum Information Processing* 18, 7 (May 2019). doi:10.1007/s11128-019-2311-9

[6] Jiayin Chen, Hendra I. Nurdin, and Naoki Yamamoto. 2020. Temporal Information Processing on Noisy Quantum Computers. *Physical Review Applied* 14, 2 (Aug. 2020). doi:10.1103/physrevapplied.14.024065

[7] Naomi Monz Chmielewski, Nina Amini, and Joseph Mikael. 2025. Quantum Reservoir Computing and Risk Bounds. doi:10.48550/ARXIV.2501.08640

[8] Sanjoy Dasgupta and Anupam Gupta. 2002. An elementary proof of a theorem of Johnson and Lindenstrauss. *Random Structures & Algorithms* 22, 1 (Nov. 2002), 60–65. doi:10.1002/rsa.10073

[9] Jérôme Dedecker, Paul Doukhan, Gabriel Lang, León R. José Rafael, Sana Louhichi, and Clémentine Prieur. 2007. *Weak Dependence: With Examples and Applications*. Springer New York. doi:10.1007/978-0-387-69952-3

[10] Paul Doukhan. 1994. *Mixing*. Springer New York. doi:10.1007/978-1-4612-2642-0

[11] Philippe Esling and Carlos Agon. 2012. Time-series data mining. *Comput. Surveys* 45, 1, Article 12 (Dec. 2012), 34 pages. doi:10.1145/2379776.2379788

[12] Keisuke Fujii and Kohei Nakajima. 2017. Harnessing Disordered-Ensemble Quantum Dynamics for Machine Learning. *Physical Review Applied* 8, 2 (Aug. 2017). doi:10.1103/physrevapplied.8.024030

[13] Marc G Genton. 2001. Classes of kernels for machine learning: a statistics perspective. *Journal of machine learning research* 2, Dec (2001), 299–312. <https://jmlr.org/papers/v2/genton01a.html>

[14] Lukas Gonon, Lyudmila Grigoryeva, and Juan-Pablo Ortega. 2020. Risk Bounds for Reservoir Computing. *Journal of Machine Learning Research* 21, 240 (2020), 1–61. <http://jmlr.org/papers/v21/19-902.html>

[15] Lyudmila Grigoryeva and Juan-Pablo Ortega. 2018. Echo state networks are universal. *Neural Networks* 108 (Dec. 2018), 495–508. doi:10.1016/j.neunet.2018.08.025

[16] Masahito Hayashi, Satoshi Ishizaka, Akinori Kawachi, Gen Kimura, and Tomohiro Ogawa. 2015. *Introduction to Quantum Information Science*. Springer Berlin Heidelberg. doi:10.1007/978-3-662-43502-1

[17] Thomas Hofmann, Bernhard Schölkopf, and Alexander J. Smola. 2008. Kernel methods in machine learning. *The Annals of Statistics* 36, 3 (june 2008). doi:10.1214/09053607000000677

[18] Fangjun Hu, Saeed A. Khan, Nicholas T. Bronn, Gerasimos Angelatos, Graham E. Rowlands, Guilhem J. Ribeill, and Hakan E. Türeci. 2024. Overcoming the coherence time barrier in quantum machine learning on temporal data. *Nature Communications* 15, 1 (Aug. 2024). doi:10.1038/s41467-024-51162-7

[19] Hsin-Yuan Huang, Michael Broughton, Masoud Mohseni, Ryan Babbush, Sergio Boixo, Hartmut Neven, and Jarrod R. McClean. 2021. Power of data in quantum machine learning. *Nature Communications* 12, 1 (May 2021). doi:10.1038/s41467-021-22539-9

[20] Hsin-Yuan (Robert) Huang, Richard Kueng, and John Preskill. 2020. Predicting Many Properties of a Quantum System from Very Few Measurements. *Nature Physics* 16, 10 (2020), 1050–1057. doi:10.1038/s41567-020-0932-7

[21] Herbert Jaeger. 2001. *The “echo state” approach to analysing and training recurrent neural networks*. Technical Report GMD Report 148. GMD—German National Research Center for Information Technology, Bonn, Germany.

[22] Herbert Jaeger. 2001. *The “echo state” approach to analysing and training recurrent neural networks*. GMD Report 148. German National Research Center for Information Technology (GMD), Sankt Augustin, Germany. <https://www.ai.rug.nl/minds/uploads/EchoStatesTechRep.pdf> Corrected version dated 2010-01-26.

[23] Ali Javadi-Abhari, Matthew Treinish, Kevin Krull, Christopher J Wood, Jake Lishman, Julien Gacon, Simon Martiel, Paul D Nation, Lev S Bishop, Andrew W Cross, et al. 2024. Quantum computing with Qiskit. *arXiv preprint arXiv:2405.08810* (2024). <https://doi.org/10.48550/arXiv.2405.08810>

[24] Tomoyuki Kubota, Yudai Suzuki, Shunpei Kobayashi, Quoc Hoan Tran, Naoki Yamamoto, and Kohei Nakajima. 2023. Temporal information processing induced by quantum noise. *Physical Review Research* 5, 2 (April 2023). doi:10.1103/physrevresearch.5.023057

[25] Rodrigo Martínez-Peña and Juan-Pablo Ortega. 2023. Quantum reservoir computing in finite dimensions. *Physical Review E* 107, 3 (March 2023). doi:10.1103/physreve.107.035306

[26] Rodrigo Martínez-Peña and Juan-Pablo Ortega. 2025. Input-dependence in quantum reservoir computing. *Physical Review E* 111, 6 (June 2025). doi:10.1103/3775-449d

[27] Boris S. Mityagin. 2015. The Zero Set of a Real Analytic Function. *arXiv:1512.07276 [math.CA]* doi:10.48550/arXiv.1512.07276

[28] Mehryar Mohri and Afshin Rostamizadeh. 2008. Rademacher complexity bounds for non-iid processes. *Advances in neural information processing systems* 21 (2008). https://proceedings.neurips.cc/paper_files/paper/2008/hash/7eab532570ff6858af2723755ff790-Abstract.html

[29] Mehryar Mohri, Afshin Rostamizadeh, and Ameet Talwalkar. 2018. *Foundations of Machine Learning* (2 ed.). The MIT Press, Cambridge, MA. <https://mitpress.mit.edu/9780262039406-foundations-of-machine-learning/>

[30] Abdelkader Mokkadem. 1988. Mixing properties of ARMA processes. *Stochastic Processes and their Applications* 29, 2 (1988), 309–315. doi:10.1016/0304-4149(88)90045-2

[31] Riccardo Molteni, Claudio Destri, and Enrico Prati. 2023. Optimization of the memory reset rate of a quantum echo-state network for time sequential tasks. *Physics Letters A* 465 (March 2023), 128713. doi:10.1016/j.physleta.2023.128713

[32] Francesco Monzani and Enrico Prati. 2025. Universality conditions of unified classical and quantum reservoir computing. *Neurocomputing* 643 (Aug. 2025), 130391. doi:10.1016/j.neucom.2025.130391

[33] Pere Mujal, Rodrigo Martínez-Peña, Gian Luca Giorgi, Miguel C. Soriano, and Roberta Zambrini. 2023. Time-series quantum reservoir computing with weak and projective measurements. *npj Quantum Information* 9 (2023), 16. doi:10.1038/s41534-023-00682-z

[34] Pere Mujal, Rodrigo Martínez-Peña, Johannes Nokkala, Jorge García-Beni, Gian Luca Giorgi, Miguel C. Soriano, and Roberta Zambrini. 2021. Opportunities in Quantum Reservoir Computing and Extreme Learning Machines. *Advanced Quantum Technologies* 4, 8 (2021). doi:10.1002/qute.202100027

[35] Pere Mujal, Rodrigo Martínez-Peña, Gian Luca Giorgi, Miguel C. Soriano, and Roberta Zambrini. 2023. Time-series quantum reservoir computing with weak and projective measurements. *npj Quantum Information* 9, 1 (Feb. 2023). doi:10.1038/s41534-023-00682-z

[36] Kohei Nakajima, Keisuke Fujii, Makoto Negoro, Kosuke Mitarai, and Masahiro Kitagawa. 2019. Boosting Computational Power through Spatial Multiplexing in Quantum Reservoir Computing. *Physical Review Applied* 11, 3 (March 2019). doi:10.1103/physrevapplied.11.034021

[37] Bernhard Schölkopf and Alexander J. Smola. 2001. *Learning with Kernels: Support Vector Machines, Regularization, Optimization, and Beyond*. The MIT Press, Cambridge, MA. doi:10.7551/mitpress/4175.001.0001

[38] Shai Shalev-Shwartz and Shai Ben-David. 2014. *Understanding Machine Learning: From Theory to Algorithms*. Cambridge University Press. doi:10.1017/cbo9781107298019

[39] Yudai Suzuki, Qi Gao, Ken C. Pradel, Kenji Yasuoka, and Naoki Yamamoto. 2022. Natural quantum reservoir computing for temporal information processing. *Scientific Reports* 12, 1 (Jan. 2022). doi:10.1038/s41598-022-05061-w

[40] V. A. Volkonskii and Yu. A. Rozanov. 1959. Some Limit Theorems for Random Functions. I. *Theory of Probability & Its Applications* 4, 2 (1959), 178–197. arXiv:<https://doi.org/10.1137/1104015> doi:10.1137/1104015

[41] David P Woodruff et al. 2014. Sketching as a tool for numerical linear algebra. *Foundations and Trends® in Theoretical Computer Science* 10, 1–2 (2014), 1–157. <https://docslib.org/doc/8200120/sketching-as-a-tool-for-numerical-linear-algebra>

[42] Toshiki Yasuda, Yudai Suzuki, Tomoyuki Kubota, Kohei Nakajima, Qi Gao, Wenzhong Zhang, Satoshi Shimono, Hendra I. Nurdin, and Naoki Yamamoto. 2023. Quantum reservoir computing with repeated measurements on superconducting devices. *ArXiv* (2023). doi:10.48550/ARXIV.2310.06706

[43] Chuanzhou Zhu, Peter J. Ehlers, Hendra I. Nurdin, and Daniel Soh. 2025. Minimalistic and scalable quantum reservoir computing enhanced with feedback. *npj Quantum Information* 11 (2025). doi:10.1038/s41534-025-01144-4

A Material related to learning-theoretic analysis

A.1 Proof of Theorem 1

Before we provide the proof of this theorem, we first describe in Section A.1.1 how a state $U^T(\mathbf{x})_t =: \rho_t$ depends on previous states in Claim 1, followed by a set-injectivity result in Proposition 1 that we leverage to establish the proof of Theorem 1.

A.1.1 Useful results.

Claim 1 (Closed form reservoir recursion). *Let $\rho_+ = |+\rangle\langle+|^{\otimes n}$ and define the input-dependent channel $\mathcal{J}_{\mathbf{x}_t}(\rho) := \mathcal{J}(\rho, \mathbf{x}_t)$ for elements \mathbf{x}_t of a window $\mathbf{x} = (x_{\tau-w+1}, \dots, x_\tau)$. Then the CEQC recursion of Eq. (9) can be written as*

$$\rho_t = \lambda \mathcal{J}_{\mathbf{x}_t}(\rho_{t-1}) + (1 - \lambda) \rho_+.$$

Define for $k \geq 1$ the backward composition operator

$$\overleftarrow{\mathcal{J}}_t^{(k)}(\rho|\mathbf{x}) := (\mathcal{J}_{\mathbf{x}_t} \circ \mathcal{J}_{\mathbf{x}_{t-1}} \circ \dots \circ \mathcal{J}_{\mathbf{x}_{t-k+1}})(\rho),$$

and for $k = 0$, $\overleftarrow{\mathcal{J}}_t^{(k)}(\rho|\mathbf{x}) := \rho$. Then the reservoir's state after consuming inputs $(x_{\tau-w+1}, \dots, x_t)$ becomes

$$\rho_t = U^T(\mathbf{x})_t = \lambda^m \overleftarrow{\mathcal{J}}_t^{(m)}(\rho_{\tau-w}|\mathbf{x}) + (1-\lambda) \sum_{k=0}^{m-1} \lambda^k \overleftarrow{\mathcal{J}}_t^{(k)}(\rho_+|\mathbf{x}), \quad (30)$$

with m being the number of applications of the evolution T : $m = t - (\tau - w) \in \{1, \dots, w\}$.

PROOF. By induction on m . The case $m = 1$ is Eq. (9). Assuming the formula holds at time $t - 1$, substitute it into $\rho_t = \lambda \mathcal{J}_{x_t}(\rho_{t-1}) + (1-\lambda)\rho_+$ and use the definition of $\overleftarrow{\mathcal{J}}_t^{(k)}$ to obtain Eq. (30). \blacksquare

Proposition 1 (Set-injectivity). *Let $\mathcal{D} = \{\mathbf{x}_1, \dots, \mathbf{x}_N\}$ be a dataset of windows. Suppose our quantum featurizer (initialized at $\rho_{-w} := |+\rangle\langle+|^{\otimes n}$) contains $R \geq 1$ sub-reservoirs that follow the design described in Section 3.1. Let our readout scheme follow the kernel-based one described in Section 3.2. Let $\epsilon_{\text{pr}}, \delta_{\text{pr}} \in (0, 1)$ be, respectively, a tolerance and a failure probability choice. Then, with a number of qubits as low as $n = \Omega\left(\epsilon_{\text{pr}}^{-2} \log\left(\frac{wN}{\delta_{\text{pr}}}\right)\right)$, we have $m \circ H^T(\mathbf{x}) \neq m \circ H^T(\mathbf{x}')$ for any pair of windows $\mathbf{x} \neq \mathbf{x}' \in \mathcal{D}$ with probability at least $1 - \delta_{\text{pr}}$.*

PROOF. In this proof, we only treat the case $R = 1$, as the cases $R > 1$ follow directly.

Let $\mathcal{P} = \bigcup_{i=1}^N \mathbf{x}_i \subset \mathbb{R}^d$ be the set that contains all points that appear inside any window, which has cardinality at most $|\mathcal{P}| \leq wN$. As described in Section 3.1.1, the event E_{JL} that describes that, for all $u, v \in \mathcal{P}$,

$$(1 - \epsilon_{\text{pr}}) \|u - v\|_2^2 \leq \|\Pi u - \Pi v\|_2^2 \leq (1 + \epsilon_{\text{pr}}) \|u - v\|_2^2,$$

has probability $\Pr(E_{\text{JL}}) \geq 1 - \delta_{\text{pr}}$ when Π follows a Gaussian Johnson–Lindenstrauss distribution as stated in Eq. (7) and $n = \Omega\left(\epsilon_{\text{pr}}^{-2} \log\left(\frac{wN}{\delta_{\text{pr}}}\right)\right)$, where the probability is over Π . Therefore, on the event E_{JL} , the map $u \mapsto \Pi u$ is injective on the set \mathcal{P} . From now on, condition on E_{JL} .

Let $\mathbf{x} = (x_{\tau-w+1}, \dots, x_\tau)$ and $\mathbf{x}' = (x'_{\tau'-w+1}, \dots, x'_{\tau'})$ be two distinct windows from the dataset \mathcal{D} . To alleviate clutter, we use the re-indexing by relative lag $t \in \{-w+1, \dots, 0\}$:

$$x_t := x_{\tau+t}, \quad x'_t := x'_{\tau'+t}.$$

Since \mathbf{x} and \mathbf{x}' are distinct, let t_\star be the latest lag where they differ:

$$t_\star := \max\{t \in \{-w+1, \dots, 0\} : x_t \neq x'_t\}.$$

Then for all $t > t_\star$, we have $x_t = x'_t$. On the event E_{JL} , Π is injective on \mathcal{P} , hence $z_{t_\star} \neq z'_{t_\star}$, where $z_t := \Pi x_t$ and $z'_t := \Pi x'_t$. In particular, there exists at least one coordinate j_\star such that $(z_{t_\star})_{j_\star} \neq (z'_{t_\star})_{j_\star}$. Additionally, injectivity of the nonlinearity $\theta(u) = \pi \tanh(u)$ preserves this difference, so that $\theta((z_{t_\star})_{j_\star}) \neq \theta((z'_{t_\star})_{j_\star})$.

Let ϑ collect all random angles in the Ising unitary as well as the parameter λ in Eq. (12). Define the “collision” condition for this window pair $(\mathbf{x}, \mathbf{x}')$ as

$$\mathcal{B}_{\mathbf{x}, \mathbf{x}'} := \{\vartheta : \Phi_\vartheta(\mathbf{x}) = \Phi_\vartheta(\mathbf{x}')\}, \quad \Phi_\vartheta(\mathbf{x}) := m \circ H^{\vartheta}(\mathbf{x}).$$

All that is left in the proof is to show that for each fixed pair $\mathbf{x} \neq \mathbf{x}'$, the set $\mathcal{B}_{\mathbf{x}, \mathbf{x}'}$ has Lebesgue measure zero. A finite union argument then yields that the union of $\mathcal{B}_{\mathbf{x}, \mathbf{x}'}$ over all $\binom{N}{2}$ pairs is still a measure-zero set; hence, with probability 1 over ϑ (since ϑ is absolutely continuous with respect to the Lebesgue measure under i.i.d. uniform sampling), no collisions occur on \mathcal{D} on the event E_{JL} .

Consider the scalar function

$$g_{\mathbf{x}, \mathbf{x}'}(\vartheta) := \|\Phi_\vartheta(\mathbf{x}) - \Phi_\vartheta(\mathbf{x}')\|_2^2.$$

Each feature coordinate $\text{Tr} [O H^{\vartheta}(\mathbf{x})]$ is obtained by composing finitely many maps that depend real-analytically on ϑ (products of single-/two-qubit rotations) with affine linear CPTP maps, and then taking a trace against a fixed observable. Hence $\Phi_\vartheta(\mathbf{x})$ and therefore $g_{\mathbf{x}, \mathbf{x}'}(\vartheta) = \|\Phi_\vartheta(\mathbf{x}) - \Phi_\vartheta(\mathbf{x}')\|_2^2$ are real-analytic in ϑ . Therefore, if we show a parameter choice ϑ^* such that $g_{\mathbf{x}, \mathbf{x}'}(\vartheta^*) > 0$, it follows from real-analyticity of $g_{\mathbf{x}, \mathbf{x}'}$ that the set $\{\vartheta : g_{\mathbf{x}, \mathbf{x}'}(\vartheta) = 0\}$ has Lebesgue measure zero (as can be found in Proposition 0 of [27]). We argue in what follows the existence of such a witness.

Let $\vartheta_\star^* = 0$. Then we have

$$V(\mathbf{x}) = \left(\bigotimes_{j=1}^n R_y(\theta(z_j)) \right).$$

As each injection qubit undergoes only Y -rotations, if the two windows differ at the latest time t_\star and projected coordinate j_\star , then the injected angles differ by

$$\Delta\theta = \underbrace{\theta((z_{t_\star})_{j_\star})}_{\alpha_{t_\star}} - \underbrace{\theta((z'_{t_\star})_{j_\star})}_{\alpha'_{t_\star}} \neq 0.$$

Since t_\star is the latest lag at which the windows differ, we have $\alpha_t = \alpha'_{t_\star}$ for all $t > t_\star$, hence the accumulated angle $\phi := \sum_{t=t_\star+1}^0 \alpha_t = \sum_{t=t_\star+1}^0 \alpha'_{t_\star}$. Consider the 1-local observables X_{j_\star} and Z_{j_\star} at the level of qubit j_\star (these belong to the feature vector since the measured set of k -local observables O contains all 1-local Paulis as discussed in Section 3.2.1). Denote the sub-vectors

$$\mu(\mathbf{x}) := \left(\langle X_{j_\star} \rangle_{\mathbf{x}}, \langle Z_{j_\star} \rangle_{\mathbf{x}} \right) \in \mathbb{R}^2, \quad \mu(\mathbf{x}') := \left(\langle X_{j_\star} \rangle_{\mathbf{x}'}, \langle Z_{j_\star} \rangle_{\mathbf{x}'} \right) \in \mathbb{R}^2.$$

Since

$$\|\mu(\mathbf{x}) - \mu(\mathbf{x}')\|_2 \neq 0 \implies \|\Phi_\vartheta(\mathbf{x}) - \Phi_\vartheta(\mathbf{x}')\|_2 \neq 0,$$

showing a witness $\lambda_\star \in (0, 1)$ for which $\mu(\mathbf{x}) - \mu(\mathbf{x}') \neq 0$ establishes the proof of the proposition. This is precisely what we show in what follows.

Leveraging the CEQC recursion defined in Claim 1, the output state $H^T(\mathbf{x})$ at lag 0 admits the expansion

$$H^T(\mathbf{x}) = \lambda^w \overleftarrow{\mathcal{J}}_0^{(w)}(\rho_{-w}|\mathbf{x}) + (1-\lambda) \sum_{k=0}^{w-1} \lambda^k \overleftarrow{\mathcal{J}}_0^{(k)}(\rho_+|\mathbf{x}),$$

where $\overleftarrow{\mathcal{J}}_0^{(k)}(\cdot|\mathbf{x})$ applies the last k encoding steps (from lags $-k+1$ up to 0) starting from state ρ . Define $i_\star := -t_\star + 1$. Because \mathbf{x} and \mathbf{x}' coincide for all lags $t > t_\star$, it follows that for all $k \leq i_\star - 1$,

$$\overleftarrow{\mathcal{J}}_0^{(k)}(\rho_+|\mathbf{x}) = \overleftarrow{\mathcal{J}}_0^{(k)}(\rho_+|\mathbf{x}').$$

Hence the final state difference $\Delta\rho_0 := H^T(\mathbf{x}) - H^T(\mathbf{x}')$ can be written as

$$\begin{aligned} \Delta\rho_0 &= \lambda^w \left(\overleftarrow{\mathcal{J}}_0^{(w)}(\rho_{-w}|\mathbf{x}) - \overleftarrow{\mathcal{J}}_0^{(w)}(\rho_{-w}|\mathbf{x}') \right) \\ &\quad + (1-\lambda) \lambda^{i_\star} \left(\overleftarrow{\mathcal{J}}_0^{(i_\star)}(\rho_+|\mathbf{x}) - \overleftarrow{\mathcal{J}}_0^{(i_\star)}(\rho_+|\mathbf{x}') \right) \\ &\quad + (1-\lambda) \sum_{k=i_\star+1}^{w-1} \lambda^k \left(\overleftarrow{\mathcal{J}}_0^{(k)}(\rho_+|\mathbf{x}) - \overleftarrow{\mathcal{J}}_0^{(k)}(\rho_+|\mathbf{x}') \right). \end{aligned} \quad (31)$$

Applying the linear map $\sigma \mapsto (\text{Tr}[X_{j_\star}\sigma], \text{Tr}[Z_{j_\star}\sigma])$ to Eq. (31) and using linearity of the trace yields

$$\mu(\mathbf{x}) - \mu(\mathbf{x}') = \lambda^w \Delta \mu_{\rho-w}^{(w)} + (1-\lambda) \lambda^{i_\star} \Delta \mu_+^{(i_\star)} + (1-\lambda) \sum_{k=i_\star+1}^{w-1} \lambda^k \Delta \mu_+^{(k)}, \quad (32)$$

where, for any $k \geq 0$ and any starting state ρ ,

$$\begin{aligned} \Delta \mu_\rho^{(k)} &:= \left(\text{Tr} \left[X_{j_\star} \tilde{\mathcal{J}}_0^{(k)}(\rho|\mathbf{x}) \right] - \text{Tr} \left[X_{j_\star} \tilde{\mathcal{J}}_0^{(k)}(\rho|\mathbf{x}') \right] \right. \\ &\quad \left. - \text{Tr} \left[Z_{j_\star} \tilde{\mathcal{J}}_0^{(k)}(\rho|\mathbf{x}) \right] + \text{Tr} \left[Z_{j_\star} \tilde{\mathcal{J}}_0^{(k)}(\rho|\mathbf{x}') \right] \right). \end{aligned}$$

As for the witness $\vartheta_\bullet^* = 0$, we have $W = \mathbb{I}$ and $\mathcal{J}_{x_t}(\rho) = V(x_t)\rho V(x_t)^\dagger$ with $V(x_t) = \bigotimes_{j=1}^n R_y(\alpha_t^{(j)})$. On qubit j_\star , starting from ρ_+ we have

$$\begin{aligned} \left(\text{Tr} \left[X_{j_\star} \tilde{\mathcal{J}}_0^{(k)}(\rho_+|\mathbf{x}) \right], \text{Tr} \left[Z_{j_\star} \tilde{\mathcal{J}}_0^{(k)}(\rho_+|\mathbf{x}) \right] \right) &= (\cos(\phi + \alpha_{t_\star}), \sin(\phi + \alpha_{t_\star})) \\ \text{and similarly with } \alpha'_{t_\star} \text{ for } \mathbf{x}'. \text{ Hence we have} \\ \|\Delta \mu_+^{(i_\star)}\|_2 &= \|(\cos(\phi + \alpha_{t_\star}), \sin(\phi + \alpha_{t_\star})) - (\cos(\phi + \alpha'_{t_\star}), \sin(\phi + \alpha'_{t_\star}))\|_2 \\ &= 2|\sin(\Delta\theta/2)| > 0. \end{aligned} \quad (33)$$

For any state σ , $|\text{Tr}[X_{j_\star}\sigma]| \leq 1$ and $|\text{Tr}[Z_{j_\star}\sigma]| \leq 1$; therefore $\|\Delta \mu_\rho^{(k)}\|_2 \leq 2\sqrt{2}$ for all k and all ρ . Using Eq. (32) and the triangle inequality gives, for $i_\star \leq w-1$,

$$\begin{aligned} \|\mu(\mathbf{x}) - \mu(\mathbf{x}')\|_2 &\geq (1-\lambda) \lambda^{i_\star} \cdot 2|\sin(\Delta\theta/2)| \\ &\quad - 2\sqrt{2}\lambda^w - 2\sqrt{2}(1-\lambda) \sum_{k=i_\star+1}^{w-1} \lambda^k. \end{aligned}$$

Since $(1-\lambda) \sum_{k=i_\star+1}^{w-1} \lambda^k \leq \lambda^{i_\star+1} - \lambda^w$, we obtain

$$\|\mu(\mathbf{x}) - \mu(\mathbf{x}')\|_2 \geq 2(1-\lambda) \lambda^{i_\star} |\sin(\Delta\theta/2)| - 2\sqrt{2}\lambda^{i_\star+1}.$$

Choosing $\lambda_\star \in (0, 1/2]$ small enough so that

$$\lambda_\star < \frac{|\sin(\Delta\theta/2)|}{\sqrt{2} + |\sin(\Delta\theta/2)|},$$

yields $\mu(\mathbf{x}) \neq \mu(\mathbf{x}')$. (If $i_\star = w$, i.e. $t_\star = -w+1$, the same computation applies with the leading contribution coming from the $\lambda^w \Delta \mu_{\rho-w}^{(w)}$ term.) This concludes the proof. \blacksquare

A.1.2 Proof of Theorem 1. Recall the setup of the K-read training in Section 3.2 where, for a fixed reservoir channel T , we learn a readout $h \in \mathcal{H}_\kappa$ by minimizing the empirical risk $\hat{R}_N(H_h^T)$ under an RKHS norm constraint $\|h\|_\kappa \leq \Lambda$, yielding an optimizer admitting a representer depending on the Gram matrix K with elements $K_{ij} = \kappa(H^T(\mathbf{x}_i), H^T(\mathbf{x}_j))$ for windows $\mathbf{x}_i, \mathbf{x}_j \in \mathcal{D}$.

Since the conditions of the theorem satisfy those of Proposition 1, the non-collision event E_{NC} , which represents “for any windows $\mathbf{x} \neq \mathbf{x}' \in \mathcal{D}$, the feature vectors $m \circ H^T(\mathbf{x})$ and $m \circ H^T(\mathbf{x}')$ do not collide”, happens with probability at least $1 - \delta_{pr}$. Condition on this event from now on.

As on E_{NC} , the vectors $m \circ H^T(\mathbf{x}_i)$ are pairwise distinct and the Matérn kernel is strictly positive definite on distinct inputs, the Gram matrix K is positive definite, hence invertible. Let the

label vector $\mathbf{y} := (y_1, \dots, y_N)^\top$, set $\boldsymbol{\alpha}^* := K^{-1}\mathbf{y}$, and consider the representer

$$h^*(\cdot) := \sum_{i=1}^N \alpha_i^* \kappa \left(H^T(\mathbf{x}_i), H^T(\cdot) \right) \in \mathcal{H}_\kappa.$$

Then we have $h^*(H^T(\mathbf{x}_i)) = (K\boldsymbol{\alpha}^*)_i = y_i$ for all i , hence $\hat{R}_N(H_{h^*}^T) = 0$. Additionally, we use $\|h^*\|_\kappa^2 = (\boldsymbol{\alpha}^*)^\top K \boldsymbol{\alpha}^* = \mathbf{y}^\top K^{-1} \mathbf{y}$ to define the threshold $\Lambda^* := \|h^*\|_\kappa = \sqrt{\mathbf{y}^\top K^{-1} \mathbf{y}} > 0$.

Fix any $\Lambda \leq \Lambda^*$ and let h_Λ be the scaled function $h_\Lambda := \frac{\Lambda}{\Lambda^*} h^*$, which yields $\|h_\Lambda\|_\kappa = \Lambda$. Using the squared loss $\ell(y, y') = (y - y')^2$ in Eq. (20) we get

$$\hat{R}_N \left(H_{h_\Lambda}^T \right) = \frac{1}{N} \sum_{i=1}^N \left(h_\Lambda(H^T(\mathbf{x}_i)) - y_i \right)^2 = \left(1 - \frac{\Lambda}{\Lambda^*} \right)^2 \frac{1}{N} \|\mathbf{y}\|_2^2.$$

Since h_Λ is feasible for the norm-constrained problem, we get that

$$\min_{h \in \mathcal{H}_\kappa(\Lambda)} \hat{R}_N(H_h^T) \leq \left(1 - \frac{\Lambda}{\Lambda^*} \right)^2 \frac{1}{N} \|\mathbf{y}\|_2^2 = O \left(\left(1 - \frac{\Lambda}{\Lambda^*} \right)^2 \right),$$

since, as assumed in Section 2.2, the labels are bounded.

Hence, with probability at least $1 - \delta_{pr}$ (that of realization of the event E_{NC}), the above inequality holds, thereby completing the proof. \blacksquare

A.2 Weakly-dependent data

In this section, we provide a quick background on β -mixing processes and outline some results that we use in our proof of Theorem 2.

A.2.1 β -mixing processes. Let $(\Omega, \mathcal{A}, \mathbb{P})$ be a probability space. For two sub- σ -algebras $\mathcal{U}, \mathcal{V} \subset \mathcal{A}$, the β -coefficient (absolute regularity coefficient) [40] is defined as

$$\beta(\mathcal{U}, \mathcal{V}) := \frac{1}{2} \sup \left\{ \sum_{i=1}^I \sum_{j=1}^J \left| \mathbb{P}(U_i \cap V_j) - \mathbb{P}(U_i) \mathbb{P}(V_j) \right| \right\}, \quad (34)$$

where the supremum is taken over all finite measurable partitions $(U_i)_i$ of Ω from \mathcal{U} and $(V_j)_j$ from \mathcal{V} . Equivalently, β can be expressed in terms of a norm in total variation [9]

$$\beta(\mathcal{U}, \mathcal{V}) = \|\mathbb{P}_{\mathcal{U} \otimes \mathcal{V}} - \mathbb{P}_{\mathcal{U}} \otimes \mathbb{P}_{\mathcal{V}}\|_{TV},$$

where $\mathbb{P}_{\mathcal{U}}, \mathbb{P}_{\mathcal{V}}$ denote restrictions of \mathbb{P} to σ -fields \mathcal{U}, \mathcal{V} and $\mathbb{P}_{\mathcal{U} \otimes \mathcal{V}}$ is a law on the product σ -field defined on rectangles by

$$\mathbb{P}_{\mathcal{U} \otimes \mathcal{V}}(U, V) = \mathbb{P}(U \cap V).$$

For a stationary random process $\mathbf{X} = (X_t)_{t \in \mathbb{Z}_-}$, the mixing coefficients are obtained as

$$\beta_{\mathbf{X}}(k) = \sup_{t^* \in \mathbb{Z}_-} \beta \left(\sigma(X_t : t \leq t^* - k), \sigma(X_t : t \geq t^*) \right),$$

where $\sigma(X_t : t)$ denotes the σ -field generated by the random process $(X_t : t)$. We say that \mathbf{X} is β -mixing if $\beta_{\mathbf{X}}(k) \xrightarrow{k \rightarrow \infty} 0$, which means that past–future dependence (regularly) converges to 0 as we increase the gap $k \in \mathbb{N}$. Furthermore, \mathbf{X} is called geometrically β -mixing if $\beta_{\mathbf{X}}(k) \leq \beta_0 e^{-\beta_1 k}$, and it is called algebraically β -mixing if $\beta_{\mathbf{X}}(k) \leq \beta_0 k^{-\beta_1}$ for some $\beta_0, \beta_1 > 0$.

A.2.2 β -mixing of the window process. Let $w \in \mathbb{N}$ be a window size, $s = w + g$ for some gap $g \in \mathbb{N}$, and $\text{IO} = ((X_t, Y_t) : t \in \mathbb{Z}_-)$ be a stationary β -mixing process. Define the windows process $\mathbf{W} = ((\mathbf{X}_\tau^w, Y_\tau) : \tau \in s\mathbb{Z}_-)$, with $s\mathbb{Z}_- := \{..., -2s, -s, 0\}$, which consists of dividing the process IO into w -sized windows

$$\mathbf{X}_\tau^w := (X_{\tau-w+1}, \dots, X_\tau) \in \mathcal{W} := (\mathcal{I})^w,$$

with indexing jumping by s .

The following result shows that the mixing coefficient $\beta_{\mathbf{W}}(k)$ of the windows process \mathbf{W} is no larger than the mixing coefficient $\beta_{\text{IO}}(ks - w)$ of the I/O process IO , which we use later on.

Claim 2 (β -mixing property of the windows process). *Let $\text{IO} = ((X_t, Y_t) : t \in \mathbb{Z}_-)$ be the I/O process and $\mathbf{W} = ((\mathbf{X}_\tau^w, Y_\tau) : \tau \in s\mathbb{Z}_-)$, with $s = w + g$, for $g \in \mathbb{N}^*$. Then we have*

$$\beta_{\mathbf{W}}(k) \leq \beta_{\text{IO}}(ks - w). \quad (35)$$

PROOF. Let $\mathbf{W} := (W_\tau : \tau \in s\mathbb{Z}_-)$ where $W_\tau := (\mathbf{X}_\tau^w, Y_\tau)$. Let $\tau^* \in s\mathbb{Z}_-$ and define the past/future σ -fields for the windows process respectively as

$$\mathcal{F}^- := \sigma(W_\tau : \tau \leq \tau^* - ks), \quad \mathcal{F}^+ := \sigma(W_\tau : \tau \geq \tau^*).$$

As each random window W_τ is measurable with respect to.

$$\sigma(IO_t : t \in \{\tau - w + 1, \dots, \tau\}),$$

with elements $IO_t := (X_t, Y_t)$, we get

$$\begin{aligned} \mathcal{F}^- &\subset \sigma(IO_t : t \leq \tau^* - ks), \quad \mathcal{F}^+ \subset \sigma(IO_t : t \geq \tau^* - w + 1) \\ &\subset \sigma(IO_t : t \geq \tau^* - w). \end{aligned}$$

We use monotonicity of $\beta(\cdot, \cdot)$ of Eq. (34) under increasing σ -fields (i.e., if $\mathcal{U} \subset \mathcal{U}'$ and $\mathcal{V} \subset \mathcal{V}'$, then $\beta(\mathcal{U}, \mathcal{V}) \leq \beta(\mathcal{U}', \mathcal{V}')$), to deduce that

$$\beta(\mathcal{F}^-, \mathcal{F}^+) \leq \beta\left(\sigma(IO_t : t \leq \tau^* - ks), \sigma(IO_t : t \geq \tau^* - w)\right)$$

Setting $t^* := \tau^* - w$ we get $\tau^* - ks = t^* - (ks - w)$. Hence, we get

$$\begin{aligned} \beta(\mathcal{F}^-, \mathcal{F}^+) &\leq \beta\left(\sigma(IO_t : t \leq t^* - (ks - w)), \sigma(IO_t : t \geq t^*)\right) \\ &\leq \beta_{\text{IO}}(ks - w), \end{aligned}$$

where the last inequality holds by definition of the β -mixing coefficients of IO . A supremum taken over t^* yields $\beta_{\mathbf{W}}(k) \leq \beta_{\text{IO}}(ks - w)$ as claimed. \blacksquare

A.2.3 Non-i.i.d. Rademacher generalization bound. As our windows dataset is built from a single realization of the underlying I/O process, the samples $\{(\mathbf{x}_i, y_i)\}_{i=1}^N$ (equivalently $\{W_\tau\}$) are in general dependent. A tractable and standard way to account for such dependence is through the β -mixing coefficients of the window process $\mathbf{W} = (W_\tau : \tau \in s\mathbb{Z}_-)$, as this mixing coefficient captures how quickly far-apart windows appear nearly independent. Non-i.i.d. Rademacher complexity bounds are specifically used for this context to characterize generalization under such setting. We provide below an adaptation of Theorem 2 of [28] to our window process \mathbf{W} .

Theorem 3 (Mohri–Rostamizadeh [28]). *Assume that $\mathbf{W} = (W_\tau : \tau \in s\mathbb{Z}_-)$ is stationary and β -mixing with coefficients $(\beta_{\mathbf{W}}(k))_{k \geq 1}$. Let \mathcal{C} be a class of measurable functions $f : \mathcal{W} \rightarrow [0, \Upsilon]$. Let $N = 2\mu$*

be an even number with $\mu \in \mathbb{N}^$. Define the total windows sample set S_N and odd-indexed windows set $S_\mu \subset S_N$ resp. as*

$$S_N := \{\mathbf{w}_{-Ns}, \dots, \mathbf{w}_{-2s}, \mathbf{w}_{-s}\}, \quad S_\mu := \{\mathbf{w}_{-(2\mu-1)s}, \dots, \mathbf{w}_{-3s}, \mathbf{w}_{-s}\}.$$

Let the statistical risk and empirical risk of a hypothesis $f \in \mathcal{C}$ be defined resp. as

$$R(f) := \mathbb{E}[f(W_0)], \quad \hat{R}_N(f) := \frac{1}{N} \sum_{i=1}^N f(\mathbf{w}_{-is}).$$

Let $\delta \in (0, 1)$ be such that $\delta > 4(\mu - 1)\beta_{\mathbf{W}}(1)$ and set

$$\delta' := \delta - 4(\mu - 1)\beta_{\mathbf{W}}(1).$$

Then, with probability at least $1 - \delta$ (over the draw of S_N), we have the following holding simultaneously for all $f \in \mathcal{C}$:

$$R(f) \leq \hat{R}_N(f) + \widehat{\mathfrak{R}}_{N/2}(C) + 3\Upsilon \sqrt{\frac{\log(4/\delta')}{N}}, \quad (36)$$

where $\widehat{\mathfrak{R}}_{N/2}(C)$ is the empirical Rademacher complexity on the subset S_μ defined as

$$\widehat{\mathfrak{R}}_{N/2}(C) := \mathbb{E}_\epsilon \left[\sup_{f \in C} \frac{2}{\mu} \left| \sum_{\mathbf{w} \in S_\mu} \epsilon_i f(\mathbf{w}) \right| \right], \quad \epsilon_i \stackrel{i.i.d.}{\sim} \text{Unif}\{\pm 1\}.$$

A.3 Proof of Theorem 2

The proof of Theorem 2 proceeds as follows.

- 1) Bound the deviation between the window risk and the empirical risk, $|R^w(H_h^T) - \hat{R}_N(H_h^T)|$, where $R^w(H_h^T)$ is the window risk given by

$$R^w(H_h^T) := \mathbb{E} \left[\ell \left(H_h^T(\mathbf{X}^w), Y \right) \right], \quad (37)$$

and where (\mathbf{X}^w, Y) is a random pair consisting of an input window of size w and its label.

- 2) Bound the deviation between the true risk and the window risk, $|R(H_h^T) - R^w(H_h^T)|$.
- 3) Finally, combine the two bounds via the triangle inequality to obtain

$$|R(H_h^T) - \hat{R}_N(H_h^T)| \leq |R(H_h^T) - R^w(H_h^T)| + |R^w(H_h^T) - \hat{R}_N(H_h^T)|.$$

A.3.1 Bounding the deviation of the window risk from the empirical one. Below we show how this deviation behaves as a direct corollary of Theorem 3.

Corollary 1 (Non-i.i.d. generalization for MSE and RKHS-ball readouts). *Let $\text{IO} = ((X_t, Y_t) : t \in \mathbb{Z}_-)$ be stationary and β -mixing, and let $s = w + g$ with $w, g \in \mathbb{N}^*$. Construct a strided windows dataset $\mathcal{D} = \{(\mathbf{x}_i, y_i)\}_{i=1}^N$ with $N = 2\mu$ even by choosing indices $t_1 > t_2 > \dots > t_N$ such that $t_i - t_{i+1} = s$. Fix a reservoir embedding H^T and a kernel κ as in Eq. (18), and consider the RKHS ball $\mathcal{H}_\kappa(\Lambda) = \{h \in \mathcal{H}_\kappa : \|h\|_\kappa \leq \Lambda\}$. Let ℓ be the squared loss $\ell(\hat{y}, y) := (\hat{y} - y)^2$. Assume the labels are bounded $|Y_t| \leq \Upsilon$ and that the kernel is normalized so that $\kappa(\rho, \rho) \leq 1$ for all ρ (respected by the Matérn profile, $\kappa(\rho, \rho) = 1$). Let the window risk $R^w(H_h^T)$ be as defined in Eq. (37). If $\delta \in (0, 1)$ satisfies*

$$\delta > 4(\mu - 1)\beta_{\text{IO}}(g), \quad \delta' := \delta - 4(\mu - 1)\beta_{\text{IO}}(g),$$

then with probability at least $1 - \delta$, the following holds simultaneously for all $h \in \mathcal{H}_\kappa(\Lambda)$:

$$\left| R^w(H_h^T) - \widehat{R}_N(H_h^T) \right| \leq \widehat{\mathfrak{R}}_{N/2}(\ell \circ \mathcal{H}_\kappa(\Lambda)) + M(N, w, g). \quad (38)$$

where $\widehat{\mathfrak{R}}_{N/2}(\ell \circ \mathcal{H}_\kappa(\Lambda))$ denotes the empirical Rademacher complexity of the loss-composed class $\ell \circ \mathcal{H}_\kappa(\Lambda)$ given by

$$\widehat{\mathfrak{R}}_{N/2}(\ell \circ \mathcal{H}_\kappa(\Lambda)) := \frac{4\Lambda(\Lambda + \Upsilon_Y)}{\sqrt{\mu}} = 4\sqrt{2} \frac{\Lambda(\Lambda + \Upsilon_Y)}{\sqrt{N}}, \quad (39)$$

and the mixing penalty $M(N, w, g)$ is given by

$$M(N, w, g) := 3(\Lambda + \Upsilon_Y)^2 \sqrt{\frac{\log(4/\delta')}{N}}. \quad (40)$$

PROOF. Let the hypothesis class $C := \{f_h : h \in \mathcal{H}_\kappa(\Lambda)\}$. By the reproducing property and the diagonal bound $\kappa(\rho, \rho) \leq 1$, we have for all $(\mathbf{x}, y) \in \mathcal{D}$

$$|h(H^T(\mathbf{x}))| \leq \|h\|_\kappa \|\kappa(H^T(\mathbf{x}), \cdot)\|_\kappa \leq \Lambda.$$

Since $|y| \leq \Upsilon_Y$, it follows that $0 \leq f_h(\mathbf{x}, y) \leq (\Lambda + \Upsilon_Y)^2$ for all (\mathbf{x}, y) , hence $C \subseteq [0, \Upsilon]^{\mathcal{W} \times \mathbb{R}}$ with $\Upsilon := (\Lambda + \Upsilon_Y)^2$.

Since $t_i - t_{i+1} = s$, the sequence $(\mathbf{w}_i)_{i=1}^N := ((\mathbf{x}_i, y_i))_{i=1}^N$ is a length- N consecutive segment of the stationary window process $\mathbf{W} = (W_\tau : \tau \in s\mathbb{Z}_-)$ (up to a deterministic time shift). Therefore, Theorem 3 applies directly to the class C with mixing coefficient $\beta_{\mathbf{W}}(1)$. Using Claim 2, we upper bound $\beta_{\mathbf{W}}(1) \leq \beta_{\mathbf{IO}}(g)$, hence $\delta' = \delta - 4(\mu - 1)\beta_{\mathbf{IO}}(g)$ and Eq. (36) yields the bound

$$R^w(H_h^T) \leq \widehat{R}_N(H_h^T) + \widehat{\mathfrak{R}}_{N/2}(C) + 3\Upsilon \sqrt{\frac{\log(4/\delta')}{N}}.$$

It remains to upper bound the empirical Rademacher complexity $\widehat{\mathfrak{R}}_{N/2}(C) = \widehat{\mathfrak{R}}_{N/2}(\ell \circ \mathcal{H}_\kappa(\Lambda))$.

Let the odd-indexed sub-dataset be $\mathcal{D}^{\text{odd}} := \{(\mathbf{x}_{2i-1}, y_{2i-1})\}_{i=1}^\mu$. By definition (Theorem 3), we have

$$\begin{aligned} \widehat{\mathfrak{R}}_{N/2}(C) &= \mathbb{E}_\epsilon \left[\sup_{h \in \mathcal{H}_\kappa(\Lambda)} \frac{2}{\mu} \left| \sum_{i=1}^\mu \epsilon_i (h(\rho_{2i-1}) - y_{2i-1})^2 \right| \right], \\ \epsilon_i &\stackrel{\text{i.i.d.}}{\sim} \text{Unif}\{\pm 1\}, \end{aligned}$$

where $\rho_{2i-1} := H^T(\mathbf{x}_{2i-1})$. Notice that for each i , the map $\psi_i(u) := (u - y_{2i-1})^2$ is L -Lipschitz on $[-\Lambda, \Lambda]$ with $L := 2(\Lambda + \Upsilon_Y)$ as we have $|\psi'_i(u)| = 2|u - y_{2i-1}| \leq 2(\Lambda + \Upsilon_Y)$. By Talagrand's lemma (see, for example, Lemma 5.7 of [29]), we have

$$\widehat{\mathfrak{R}}_{N/2}(C) \leq 2(\Lambda + \Upsilon_Y) \widehat{\mathfrak{R}}_{N/2}(\mathcal{H}_\kappa(\Lambda)),$$

$$\text{where } \widehat{\mathfrak{R}}_{N/2}(\mathcal{H}_\kappa(\Lambda)) := \mathbb{E}_\epsilon \left[\sup_{h \in \mathcal{H}_\kappa(\Lambda)} \frac{2}{\mu} \left| \sum_{i=1}^\mu \epsilon_i h(\rho_{2i-1}) \right| \right].$$

$\widehat{\mathfrak{R}}_{N/2}(\mathcal{H}_\kappa(\Lambda))$ is the empirical Rademacher complexity of the RKHS ball $\mathcal{H}_\kappa(\Lambda)$ which, by the reproducing property of the kernel κ

together with Cauchy-Schwarz, satisfies

$$\begin{aligned} \widehat{\mathfrak{R}}_{N/2}(\mathcal{H}_\kappa(\Lambda)) &\leq \frac{2\Lambda}{\mu} \mathbb{E}_\epsilon \left[\left\| \sum_{i=1}^\mu \epsilon_i \kappa(\rho_{2i-1}, \cdot) \right\|_\kappa \right] \\ &\leq \frac{2\Lambda}{\mu} \sqrt{\mathbb{E}_\epsilon \left[\left\| \sum_{i=1}^\mu \epsilon_i \kappa(\rho_{2i-1}, \cdot) \right\|_\kappa^2 \right]} \\ &= \frac{2\Lambda}{\mu} \sqrt{\mathbb{E}_\epsilon [\epsilon^\top K \epsilon]} = \frac{2\Lambda}{\mu} \sqrt{\text{Tr}[K]}, \end{aligned}$$

where $\epsilon := (\epsilon_1, \dots, \epsilon_\mu)^\top \in \{\pm 1\}^\mu$, K is the Gram matrix

$$K = (\kappa(\rho_{2i-1}, \rho_{2j-1}))_{i,j},$$

and the equality $\mathbb{E}_\epsilon [\epsilon^\top K \epsilon] = \text{Tr}[K]$ follows from independence and $\mathbb{E}[\epsilon_i \epsilon_j] = \delta_{ij}$. Again, as κ is norm-diagonal, we have $\text{Tr}[K] \leq \mu$, hence $\widehat{\mathfrak{R}}_{N/2}(\mathcal{H}_\kappa(\Lambda)) \leq \frac{2\Lambda}{\sqrt{\mu}}$, which yields in turn

$$\widehat{\mathfrak{R}}_{N/2}(C) \leq \frac{4\Lambda(\Lambda + \Upsilon_Y)}{\sqrt{\mu}}.$$

■

A.3.2 Bounding the deviation of the window risk from the statistical one. Before stating a bound for such a deviation, we first show a geometric decaying of the dependence of the reservoir output on the far past, which is related to the exponentially fading memory property of our reservoir.

Proposition 2 (Geometric decay of dependence of reservoir outputs on inputs). *Let $\mathbf{x} = (x_t : t \in \mathbb{Z}_-) \in (\mathcal{I})^{\mathbb{Z}_-}$ be a time series, and let $\mathbf{x}^w := (x_{-w+1}, \dots, x_0) \in (\mathcal{I})^w$ be its last truncated window. Let H_h^T be a QUARK reservoir as described in Section 3 where H^T is composed of $R \geq 1$ sub-reservoirs each of contraction factor λ_r , \mathcal{O} are the k -local observables measured per sub-reservoir, and $h \in \mathcal{H}_\kappa(\Lambda)$, where κ is a Matérn-based kernel as defined in Eq. (18) parameterized on $v > 1$, and $\xi > 0$. Then we have*

$$|H_h^T(\mathbf{x}) - H_h^T(\mathbf{x}^w)| \leq \frac{2\Lambda}{\xi} \sqrt{\frac{vR|\mathcal{O}|}{v-1}} \lambda_\star^w, \quad (41)$$

where $\lambda_\star := \max_r \lambda_r$, and the reservoir is initialized for the finite window case to an arbitrary state $\rho'_w \in \mathcal{S}(\mathcal{H})^R$.

PROOF. Let the sequence of states produced by the reservoir via consuming the full time series and the truncated window be respectively

$$U^T(\mathbf{x}) := (\rho_t \in \mathcal{S}(\mathcal{H})^R : t \in \mathbb{Z}_-),$$

$$U^T(\mathbf{x}^w) := (\rho'_t \in \mathcal{S}(\mathcal{H})^R : t \in \{-w+1, \dots, 0\}),$$

where, by definition, the truncated evolution $(U^T(\mathbf{x}^w))_{-w}$ is initialized at some state $\rho'_{-w} \in \mathcal{S}(\mathcal{H})^R$, and both $U^T(\mathbf{x})$ and $U^T(\mathbf{x}^w)$ are then driven by the same input sequence over the last w time steps.

Since the composed reservoir $T(\rho, x)$ is λ_\star -contractive with respect to the trace norm $\|\cdot\|_1$, with $\lambda^\star := \max_r \lambda_r$, we have

$$\begin{aligned} \|\rho_0 - \rho'_0\|_1 &\leq \lambda_\star \|\rho_{-1} - \rho'_{-1}\|_1 \\ &\leq \lambda_\star^2 \|\rho_{-2} - \rho'_{-2}\|_1 \\ &\vdots \\ &\leq \lambda_\star^w \|\rho_{-w} - \rho'_{-w}\|_1 \leq 2\lambda_\star^w, \end{aligned} \quad (42)$$

where the last inequality leverages the fact that the diameter of the space of density operators is 2 with respect to the trace norm.

We now account for the readout. By definition, we have

$$|H_h^T(\mathbf{x}) - H_h^T(\mathbf{x}^w)| = |h(\rho_0) - h(\rho'_0)|.$$

Using the reproducing property in \mathcal{H}_κ we get

$$\begin{aligned} |h(\rho_0) - h(\rho'_0)| &= |\langle h, \kappa(\rho_0, \cdot) - \kappa(\rho'_0, \cdot) \rangle_\kappa| \\ &\leq \|h\|_\kappa \|\kappa(\rho_0, \cdot) - \kappa(\rho'_0, \cdot)\|_\kappa, \end{aligned} \quad (43)$$

with $\langle \cdot, \cdot \rangle_\kappa$ being the RKHS inner product. Furthermore, we have

$$\begin{aligned} \|\kappa(\rho_0, \cdot) - \kappa(\rho'_0, \cdot)\|_\kappa^2 &= \kappa(\rho_0, \rho_0) + \kappa(\rho'_0, \rho'_0) - 2\kappa(\rho_0, \rho'_0) \\ &= 2 \left(\varphi(0) - \varphi \left(\|m(\rho_0) - m(\rho'_0)\|_2 \right) \right), \end{aligned} \quad (44)$$

where Eq. (18) was used. Define the constant

$$L_\kappa := \sup_{s>0} \frac{\sqrt{2(\varphi(0) - \varphi(s))}}{s}.$$

We show in the next paragraph that $L_\kappa \leq \sqrt{-\varphi''(0)}$, where $\varphi''(0)$ is the second derivative of φ at the origin, which exists for the Matérn profile φ as $v > 1$ (i.e., $\varphi \in C^2$ at 0).

To show that $L_\kappa \leq \sqrt{-\varphi''(0)}$, we use the standard Bochner [17] result stating that for stationary covariance (kernel) functions such as $\psi(\eta) := \varphi(\|\eta\|_2)$, there exists a finite nonnegative symmetric spectral measure γ such that

$$\psi(\eta) = \int_{\mathbb{R}^d} e^{i\omega^\top \eta} d\gamma(\omega) = \int_{\mathbb{R}^d} \cos(\omega^\top \eta) d\gamma(\omega),$$

where the last equality holds as ψ is real and even. Hence we have

$$\varphi(0) - \varphi(\|\eta\|_2) = \psi(0) - \psi(\eta) = \int_{\mathbb{R}^d} (1 - \cos(\omega^\top \eta)) d\gamma(\omega).$$

Using the elementary inequality $1 - \cos t \leq t^2/2$ (valid for all t) yields

$$\begin{aligned} \varphi(0) - \varphi(\|\eta\|_2) &\leq \frac{1}{2} \int_{\mathbb{R}^d} (\omega^\top \eta)^2 d\gamma(\omega) \\ &\leq \frac{\|\eta\|_2^2}{2} \int_{\mathbb{R}^d} (\omega^\top e)^2 d\gamma(\omega), \quad e := \frac{\eta}{\|\eta\|_2}. \end{aligned} \quad (45)$$

Consider the 1D restriction $g(t) = \psi(te) = \varphi(|t|)$. Differentiating the spectral representation twice at point $t = 0$ (legitimate as $\varphi''(0)$ exists), we get

$$g''(0) = \frac{d^2}{dt^2} \int \cos(t\omega^\top e) d\gamma(\omega) \Big|_{t=0} = - \int (\omega^\top e)^2 d\gamma(\omega) = -\varphi''(0),$$

where the last equality holds as $g''(0) = \varphi''(0)$. The last inequality of Eq. (45) therefore yields $2(\varphi(0) - \varphi(s)) \leq -\varphi''(0)s^2$, which directly leads to

$$L_\kappa \leq \sqrt{-\varphi''(0)}. \quad (46)$$

Hence setting $s = \|m(\rho_0) - m(\rho'_0)\|_2$ yields

$$\begin{aligned} \sqrt{2 \left(\varphi(0) - \varphi \left(\|m(\rho_0) - m(\rho'_0)\|_2 \right) \right)} &\leq L_\kappa \|m(\rho_0) - m(\rho'_0)\|_2 \\ &\leq \|m(\rho_0) - m(\rho'_0)\|_2 \sqrt{-\varphi''(0)}. \end{aligned}$$

Furthermore, let $z := \sqrt{2v}s/\xi$ so that the Matérn profile (defined in Eq. (17)) becomes

$$\varphi(s) = \frac{2^{1-v}}{\Gamma(v)} z^v K_v(z).$$

For $v > 1$, the small- z expansion of K_v gives

$$z^v K_v(z) = 2^{v-1} \Gamma(v) \left(1 + \frac{z^2}{4(1-v)} + O(z^4) \right) \quad (z \rightarrow 0).$$

Substituting into the definition of φ yields

$$\varphi(s) = 1 - \frac{1}{4(v-1)} z^2 + O(z^4) = 1 - \frac{v}{2(v-1)\xi^2} s^2 + O(s^4).$$

Hence $\varphi''(0) = -\frac{v}{(v-1)\xi^2}$, i.e.,

$$-\varphi''(0) = \frac{1}{\xi^2} \frac{v}{v-1}.$$

Therefore, from Eq. (46) we get $L_\kappa \leq \frac{1}{\xi} \sqrt{\frac{v}{v-1}}$, and hence, combining Eq. (43) and Eq. (44), we get

$$\begin{aligned} |h(\rho_0) - h(\rho'_0)| &\leq \|h\|_\kappa \|\kappa(\rho_0, \cdot) - \kappa(\rho'_0, \cdot)\|_\kappa \\ &\leq \|h\|_\kappa L_\kappa \|m(\rho_0) - m(\rho'_0)\|_2 \\ &\leq \|h\|_\kappa \frac{1}{\xi} \sqrt{\frac{v}{v-1}} \|m(\rho_0) - m(\rho'_0)\|_2. \end{aligned} \quad (47)$$

Finally, for the moment map $m(\rho) = (\text{Tr}[O_\ell \rho])_{\ell=1}^{R|\mathcal{O}|}$, where $R|\mathcal{O}|$ is the number of observables measured across all sub-reservoirs, and where each O_ℓ is formed from a k -local observable (from \mathcal{O}) padded by identities to act on the full space $\mathcal{S}(\mathcal{H})^R$ (this does not change the operator norm), we have for each ℓ by Hölder's inequality for Schatten norms

$$|\text{Tr}[O_\ell(\rho_0 - \rho'_0)]| \leq \|O_\ell\|_\infty \|\rho_0 - \rho'_0\|_1. \quad (48)$$

As the operator norm of a Pauli string satisfies $\|O_\ell\|_\infty = 1$, we get

$$\|m(\rho_0) - m(\rho'_0)\|_2 = \left(\sum_{\ell=1}^{R|\mathcal{O}|} |\text{Tr}[O_\ell(\rho_0 - \rho'_0)]|^2 \right)^{1/2} \leq \sqrt{R|\mathcal{O}|} \|\rho_0 - \rho'_0\|_1. \quad (49)$$

Combining Eqs. (42), (47), and (49), along with the fact that $\|h\|_\kappa \leq \Lambda$, we get the claimed bound

$$|h(\rho_0) - h(\rho'_0)| \leq \frac{\Lambda}{\xi} \sqrt{\frac{v}{v-1}} \cdot \sqrt{R|\mathcal{O}|} \|\rho_0 - \rho'_0\|_1 \leq \frac{2\Lambda}{\xi} \sqrt{\frac{vR|\mathcal{O}|}{v-1}} \lambda_\star^w. \quad \blacksquare$$

We now provide the bound on the deviation $|R(H_h^T) - R^w(H_h^T)|$.

Corollary 2 (Deviation of the window risk from the statistical one). *Let the conditions of Proposition 2 apply, with the additional assumption that the considered time series is drawn from the stationary process $\text{IO} = ((X_t, Y_t) : t \in \mathbb{Z}_-)$ and that the outputs satisfy $|Y_t| \leq Y_Y$. Then we have*

$$|R(H_h^T) - R^w(H_h^T)| \leq \frac{4\Lambda(\Lambda + Y_Y)}{\xi} \sqrt{\frac{vR|\mathcal{O}|}{v-1}} \lambda_\star^w. \quad (50)$$

PROOF. We have

$$R(H_h^T) - R^w(H_h^T) = \mathbb{E} \left[\ell \left(H_h^T(\mathbf{X}), Y_0 \right) \right] - \mathbb{E} \left[\ell \left(H_h^T(\mathbf{X}_0^w), Y_0 \right) \right],$$

where by stationarity we write $\mathbf{X} = (\dots, X_{-w-1}, X_{-w}, \mathbf{X}_0^w)$. Hence we get

$$\begin{aligned} |R(H_h^T) - R^w(H_h^T)| &= \left| \mathbb{E} \left[\ell \left(H_h^T(\mathbf{X}), Y_0 \right) - \ell \left(H_h^T(\mathbf{X}_0^w), Y_0 \right) \right] \right| \\ &\leq \mathbb{E} \left[\left| \ell \left(H_h^T(\mathbf{X}), Y_0 \right) - \ell \left(H_h^T(\mathbf{X}_0^w), Y_0 \right) \right| \right] \\ &\leq \mathbb{E} \left[L \left| H_h^T(\mathbf{X}) - H_h^T(\mathbf{X}_0^w) \right| \right] \\ &\leq L \frac{2\Lambda}{\xi} \sqrt{\frac{vR|O|}{v-1}} \lambda_\star^w, \end{aligned}$$

where the last inequality uses that the squared loss is L -Lipschitz on $[-\Lambda, \Lambda] \times [-\Upsilon_Y, \Upsilon_Y]$, with $L := 2(\Lambda + \Upsilon_Y)$ (see the third paragraph of the proof of Corollary 1), together with Proposition 2. \blacksquare

We finally are now ready to provide proof of Theorem 2.

A.3.3 Proof of Theorem 2. Since conditions of Theorem 2 satisfy both conditions of Corollary 1 and Corollary 2, and from

$$|R(H_h^T) - R_N(H_h^T)| \leq |R(H_h^T) - R^w(H_h^T)| + |R^w(H_h^T) - R_N(H_h^T)|,$$

we conclude that

$$|R(H_h^T) - R_N(H_h^T)| \leq \widehat{\mathfrak{R}}_{N/2}(\ell \circ \mathcal{H}_\kappa(\Lambda)) + M(N, w, g, \delta') + G(h, \Lambda, T)$$

where $\widehat{\mathfrak{R}}_{N/2}(\ell \circ \mathcal{H}_\kappa(\Lambda))$ denotes the empirical Rademacher complexity of the loss-composed class $\ell \circ \mathcal{H}_\kappa(\Lambda)$ given by

$$\widehat{\mathfrak{R}}_{N/2}(\ell \circ \mathcal{H}_\kappa(\Lambda)) := 4\sqrt{2} \frac{\Lambda(\Lambda + \Upsilon_Y)}{\sqrt{N}},$$

the mixing penalty $M(N, w, g)$ given by

$$M(N, w, g) := 3(\Lambda + \Upsilon_Y)^2 \sqrt{\frac{\log(4/\delta')}{N}}$$

and the window truncation geometrically decaying penalty given by

$$\mathfrak{G}(\kappa, \Lambda, T) := \frac{4\Lambda(\Lambda + \Upsilon_Y)}{\xi} \sqrt{\frac{vR|O|}{v-1}} \lambda_\star^w. \quad \blacksquare$$

B Additional details for numerical validation

In this appendix, we provide further details on the data generation process and target functionals used in the numerical experiments.

B.1 Data generation.

B.1.1 Input VARMA process.

Definition. Let $\mathbf{X} := (X_t : t \in \mathbb{Z}_-)$ be a (strictly) stationary VARMA(p, q) process (sometimes called VARMA for vector VARMA), i.e.,

$$X_t = \sum_{i=1}^p \Phi_i X_{t-i} + \Theta_0 \epsilon_t + \sum_{j=1}^q \Theta_j \epsilon_{t-j}, \quad (51)$$

where $(\epsilon_t)_{t \in \mathbb{Z}_-}$ are i.i.d. centred innovations with $\mathbb{E}[\|\epsilon_t\|_2^2] < \infty$, and Φ_i, Θ_j are $d \times d$ matrices, with Θ_0 non singular. Define the lag operator $LX_t := X_{t-1}$, and set the matrix polynomials

$$\Phi(L) := I_d - \sum_{i=1}^p \Phi_i L^i, \quad \Theta(L) := \Theta_0 + \sum_{j=1}^q \Theta_j L^j,$$

then the model in Eq. (51) is $\Phi(L)X_t = \Theta(L)\epsilon_t$. It is shown in [30] that if the innovations $(\epsilon_t)_{t \in \mathbb{Z}_-}$ are i.i.d. with a distribution absolutely continuous with respect to the Lebesgue measure on \mathbb{R}^d (i.e. admitting a density), and if the AR polynomial is stable (i.e. the VARMA is causal), namely

$$\det(I_d - \sum_{i=1}^p \Phi_i z^i) \neq 0, \quad \forall z \in \mathbb{C}, |z| \leq 1, \quad (52)$$

together with the non-degeneracy condition of $\det(\Theta_0) \neq 0$, then the strictly stationary unique solution of Eq. (51) is (in fact geometrically) β -mixing.

Experimental setting (stable VARMA(p, q) family). Fix $(d, p, q) \in \mathbb{N}^* \times \mathbb{N}^* \times \mathbb{N}$ and choose a stability budget $\gamma \in (0, 1)$ (which controls the dependence strength: larger γ yields slower mixing). We generate a random stable VAR part as follows. Draw i.i.d. matrices $(\Phi_i)_{i=1}^p$ with entries $\sim \mathcal{N}(0, 1)$ and define the normalized directions $U_i := \Phi_i / \|\Phi_i\|_2$. Draw i.i.d. positive weights $w_i \sim \text{Unif}(0, 1)$ and set $a_i := \gamma w_i / \sum_{k=1}^p w_k$, so that $\sum_{i=1}^p a_i = \gamma$. Finally set

$$\Phi_i := a_i U_i, \quad i = 1, \dots, p,$$

which ensures $\sum_{i=1}^p \|\Phi_i\|_2 = \gamma < 1$ and therefore the AR-stability (causality) condition

$$\det(I_d - \sum_{i=1}^p \Phi_i z^i) \neq 0, \quad \text{for all } |z| \leq 1.$$

For the MA part, we take $\Theta_0 := I_d$ (hence nonsingular) and generate $\Theta_j := b_j V_j$ for $j = 1, \dots, q$, where $V_j := \tilde{\Theta}_j / \|\tilde{\Theta}_j\|_2$ with $\tilde{\Theta}_j$ i.i.d. Gaussian matrices and where $(b_j)_{j=1}^q$ are decaying amplitudes, e.g. $b_j := \eta \rho^{j-1}$ with $\eta > 0$ and $\rho \in (0, 1)$. The innovations $(\epsilon_t)_{t \in \mathbb{Z}_-}$ are i.i.d. with a Lebesgue density on \mathbb{R}^d , for instance $\epsilon_t \sim \mathcal{N}(0, \sigma^2 I_d)$.

We simulate the (unbounded) VARMA recursion

$$Z_t = \sum_{i=1}^p \Phi_i Z_{t-i} + \Theta_0 \epsilon_t + \sum_{j=1}^q \Theta_j \epsilon_{t-j}$$

with a burn-in $B \gg 1$ and retain the last T samples. To match the bounded input set $\mathcal{I} = (-1, 1)^d$ used in the main experiments, we finally set

$$X_t := \tanh(Z_t) \in (-1, 1)^d \quad (\text{componentwise}).$$

Since X_t is a measurable transformation of Z_t , it inherits the (geometric) β -mixing property of the VARMA process.

B.2 Output processes (functionals)

To obtain scalar labels $Y_t \in \mathbb{R}$ from vector inputs $X_t \in (-1, 1)^d$, we consider three real-valued fading-memory functionals $H^\star : (\mathcal{I})^{\mathbb{Z}_-} \rightarrow \mathbb{R}$ evaluated on the past orbit $X_t := (X_{t-k})_{k \geq 0}$. Throughout, we fix a window size $w \in \mathbb{N}^*$ and use the window-truncated evaluation $H_w^\star(X_t)$, obtained by restricting $k \in \{0, \dots, w-1\}$.

Random projection vectors. We generate a random unit vector $u \in \mathbb{R}^d$ by drawing $g \sim \mathcal{N}(0, I_d)$ and setting

$$u := \frac{g}{\|g\|_2}. \quad (53)$$

When needed, we generate $v \in \mathbb{R}^d$ independently the same way and (optionally) orthogonalize it via

$$\tilde{v} := v - \langle v, u \rangle u, \quad v := \frac{\tilde{v}}{\|\tilde{v}\|_2}. \quad (54)$$

This choice ensures u (and v) are uniformly distributed on the unit sphere \mathbb{S}^{d-1} .

(F1) Scalar one-step forecasting. Fix u as in Eq. (53) and define the forecasting functional

$$H_{\text{fore}}^*(X_t) := u^\top X_{t+1}, \quad Y_t := H_{\text{fore}}^*(X_t). \quad (55)$$

(F2) Exponentially fading linear functional. Fix u as in Eq. (53) and a decay $\alpha \in (0, 1)$. Define

$$H_{\text{exp}}^*(X_t) := \sum_{k=0}^{\infty} \alpha^k u^\top X_{t-k}, \quad Y_t := H_{\text{exp},w}^*(X_t) := \sum_{k=0}^{w-1} \alpha^k u^\top X_{t-k}. \quad (56)$$

(F3) Truncated Volterra fading-memory functional (order 2).

Fix u, v as in Eq. (53)–Eq. (54) and a decay $\alpha \in (0, 1)$. We define a (causal) Volterra functional of order 2 with exponentially decaying kernels,

$$H_{\text{vol}}^*(X_t) := \sum_{k=0}^{\infty} h_1(k)^\top X_{t-k} + \sum_{k=0}^{\infty} \sum_{\ell=0}^{\infty} X_{t-k}^\top H_2(k, \ell) X_{t-\ell}, \quad (57)$$

where we take the rank-one fading kernels

$$h_1(k) := \alpha^k u, \quad H_2(k, \ell) := \frac{1}{2} \alpha^{k+\ell} v v^\top, \quad (58)$$

so that

$$H_{\text{vol}}^*(X_t) = \sum_{k=0}^{\infty} \alpha^k u^\top X_{t-k} + \frac{1}{2} \sum_{k=0}^{\infty} \sum_{\ell=0}^{\infty} \alpha^{k+\ell} (v^\top X_{t-k})(v^\top X_{t-\ell}). \quad (59)$$

In experiments, we use the window-truncated version

$$Y_t := H_{\text{vol},w}^*(X_t) := \sum_{k=0}^{w-1} \alpha^k u^\top X_{t-k} + \frac{1}{2} \sum_{k=0}^{w-1} \sum_{\ell=0}^{w-1} \alpha^{k+\ell} (v^\top X_{t-k})(v^\top X_{t-\ell}). \quad (60)$$

Since $X_t \in (-1, 1)^d$ and $\alpha \in (0, 1)$, all targets are bounded.

B.3 Kernel hyper-parameters tuning

For each task, we select the Matérn kernel hyper-parameters once using a lightweight train/validation procedure, and then keep them fixed across all reported runs for that task. The tuner is intentionally simple (single split and basic optimizers) to keep the overhead minimal compared to the cost of quantum feature.

Setup. Given a dataset of quantum features and targets $\{(z_i, y_i)\}_{i=1}^N$ with $Z \in \mathbb{R}^{N \times D}$ and $y \in \mathbb{R}^N$, we create a validation split by shuffling indices with a fixed seed and allocating a fraction `val_ratio` = 0.2 to validation. During hyper-parameter tuning, we fix a small ridge term $\lambda_{\text{reg}} = 10^{-6}$ to stabilize the Gram-matrix inversion while focusing the search on the kernel shape.

Objective (validation MSE). For candidate Matérn hyper-parameters (ξ, v) (length-scale and smoothness), we evaluate the validation mean-squared error of kernel ridge regression (KRR). Concretely, we compute

$$\hat{y}_{\text{val}} = K_{\text{val}, \text{tr}} \alpha, \quad \alpha = (K_{\text{tr}, \text{tr}} + \lambda_{\text{reg}} I)^{-1} y_{\text{tr}},$$

where $K_{\text{tr}, \text{tr}} = [\kappa_{\xi, v}(z_i, z_j)]_{i, j \in \text{tr}}$ and $K_{\text{val}, \text{tr}} = [\kappa_{\xi, v}(z_i, z_j)]_{i \in \text{val}, j \in \text{tr}}$. The objective is $\text{MSE}(y_{\text{val}}, \hat{y}_{\text{val}})$.

Grid over v and bounded search over ξ . We adopt the grid tuning strategy: we scan a small candidate set of smoothness values

$$v \in \{0.5, 1.5, 2.5, 5.0\},$$

and, for each fixed v , we solve the one-dimensional problem

$$\xi^*(v) \in \arg \min_{\xi \in [10^{-3}, 10^3]} \text{MSE}_{\text{val}}(\xi, v),$$

using bounded optimization in $\log(\xi)$ (maximum `xi_maxiter`=80 iterations). We then select the final pair as

$$(\xi^*, v^*) \in \arg \min_{(\xi^*(v), v)} \text{MSE}_{\text{val}}(\xi^*(v), v),$$

and store (ξ^*, v^*) as the task-level Matérn kernel configuration.